공학박사 학위논문

Mechanical analysis of three dimensional textile composites using fiber-based continuum model

섬유기반 연속체 모델을 이용한 삼차원 텍스타일 복합재료의 역학적 해석

2016년 2월

서울대학교 대학원

재료공학부

안 현 철

Mechanical analysis of three dimensional textile composites using fiber-based continuum model

Advisor: Woong-Ryeol Yu

by

Hyunchul Ahn

2016

Department of Materials Science and Engineering
Graduated School
Seoul National University

Abstract

Fiber reinforced polymer composites are widely used in industrial field, such as military, aerospace and automobile, and in the spotlight of using structural materials. For this reason, mechanical analysis and manufacturing process composites are researched in numerus studies. Moreover, many structural analysis of composites are published for improving its properties and reinforcing its properties. Unit cell approach is major concept of mechanical analysis of composite and three dimensional (3D) modelling of composite structure is well established. This unit cell analysis has high accuracy and reflecting complicated composite structures, however it has high cost of computing time and modeling process. Moreover it cannot be considered structural effect from deformation and loading condition. For this reason, new approach of composite mechanical analysis is developed with continuum based model in this study. The aim of this method is continuum analysis with fast computing time and considering structural effect of textile composite structures with one-step 3D structural analysis.

New numerical analysis model, called fiber based continuum model (FBM), is continuum based algorithm considered fiber orientation and structure of a textile composite. Fiber architecture is important factor of mechanical properties of a composite, so FBM is focused on fiber structure and its change inside of a composite. Moreover, this method is used fiber and matrix properties for numerical analysis, so structural analysis can be done with minimum parameters. Furthermore, based on layer method and modified ply discount method, Failure behavior can be predicted with Puck's failure citation.

3D textile composite fabrication and structure analysis method are developed for numerical validation and characterization, in the next chapter. FBM analysis can be used for arbitrary 3D textile composites with yarn path function, so verification works is needed with several 3D structures. In this study, 3D five axis braided and orthogonal woven composite is manufactured and tested. For this, 3D weaving method was developed in laboratory scale. Moreover, before the mechanical test of composites, structural analysis is done with micro-CT image.

Finally, FBM is verified with experimental of 3D textile composites. Tensile and bending test was done for characterization of composites. The experimental results of which were compared with simulated results, demonstrating that the current numerical model can properly predict the mechanical behavior of 3D fiber-reinforced composites. Moreover, based on FBM analysis, application of 3D textile composite is investigated.

Keywords: fiber-reinforced composites, numerical analysis, structural analysis, 3D composites, fiber based model

Student Number: 2010-30177

Contents

List of Figures

List of Tables

Chapter 1. Introduction

1.1 Fiber reinforced polymer composites (FRPs)

Fiber reinforced polymer composites (FRPs) have been widely used such as sports goods and structural materials, because of their high stiffness and strength. Woven and braided composite are typical types of fiber reinforced composite, showing high mechanical performance. FRPs prove durability and stability of the material in these days so designers and manufacturers used FRPs in very sophisticated and highly loaded structures. Especially, carbon fiber is one of strongest fiber in the area and it is a material consisting of fibers about around 10 micrometers in diameter. Carbon fibers have higher properties such as high stiffness, high tensile strength, light weight, and high thermal, chemical resistance than similar fibers as glass or plastic fibers. This carbon fiber are usually manufactured composite with other resin materials and carbon fiber reinforced polymer composite (CFRP) is widely used because it has extremely high strength-to-weight ratio. Also, it is used with other compound for particular object such as carbon-carbon composites for high temperature atmosphere.

FRPs have numerus structures from simple unidirectional composite to 3D complex structures. Fundamental FRP structure is unidirectional composites and it is used many industrial field with laminate structures. It is one dimensional (1D) structure and has high stiffness according to longitudinal direction, however it has extremely anisotropic properties and delamination

problems so other structures are developed and researched. Next part is two dimensional (2D) structures such as woven and braided composites, it can be controlled plane properties so used for many sheet and plate structures as laminate composites.

Woven structure is most commonly used form of textile composite for structural application. It is generally consist of warp and weft yarns those are longitudinal and transverse direction to the yarn orientation. Woven structure has several structures according to these yarn orientation and interaction such as plain, twill and satin weaves which are classified by repeating patterns. Plain weave is basic structures of 2D woven and its repeating unit is one warp yarn and one weft yarn. Twill and satin weaves are over one warp yarns for one weft yarn in the repeating units. Woven fabrics also can be classified by opened-packing and closed-packings [1]. This classification is based on gaps between two yarns in warp or weft. This woven structures have good stability and reliability for structural materials as sheet and plate however poor properties on in-plane shear. Braided fabrics are used more high-end application of FRPs. Braided structures are constructed by intertwining of two or more set of yarns. Also axial yarns, which is aligned longitudinal direction for reinforcing stiffness of braided structure, is used for tri-axial braided composite and this composite used for high-end industries such as aircraft and military. Braiding structure has also several variations with braiding parameters as woven fabrics and it can be manipulated mechanical properties more than other 2D textile composites such as braid angle, yarn size, yarn spacing, and fiber volume fractions.

However 1D or 2D structures cannot be overcome delamination and torsional problems so 3D FRPs are developed and researched based on 2D structures such as 3D braided and 3D woven composites. These 3D composites have no delamination, high failure strength, and long fatigue life. So using 3D composites for structural materials, many studies was done and still researching in these days. For researching FRPs properties, numerical analysis is usually adopted because complex FRP structures have many parameters for mechanical behavior of the composites.

1.2 Mechanical behavior prediction of FRPs

1.2.1 Composite stiffness prediction theories

The mechanical analysis of the composites has been well developed using numerical methods in many studies and well established in many works [1, 2]. Finite element method has been used universally for numerical analysis of structural problems and it is also for FRPs analysis. Here, FRPs have repeating units and inner yarn structures so the general procedure of analysis the mechanical properties of composite is unit cell determination and its reconstruction with periodic boundary condition. Therefore, mechanical properties prediction is depends on unit cell modelling and assembled composite structures.

For woven composites, it is conventional structure and is has been researched several decades. First conventional analytical method was developed by Ishikawa, T. and Chou, T. W. with linear and nonlinear model for stiffness and

strength of woven composites [3, 4]. This model, called mosaic model, is developed for analysis and the textile composite is simply regarded as assemble of pieces of cross-ply laminate (see Figure ….). In this model the shear deformation in the thickness direction is neglected and a lamina was simplified to two 1D approach. The lamination plate theory is used for calculate the mechanical stiffness and compliances. This model has good agreement between predictions and experimental results, however fiber continuity and stress and strain in the interlaced region were not considered. Therefore, crimp model, called fiber undulation model, was proposed [4]. This model contained fiber continuity and undulation of the yarn in the 'mosaic model'. These model were very useful for understanding and predicting mechanical properties of woven fabrics. Moreover, 'bridge model' was developed for considering interaction between an undulated regions and it was applied to analysis non-linear behavior of textile composites such as Hahn and Tsai model [5]. Whitney and Chou [6] developed a new model to predict elastic properties of composites reinforced with 3D angle interlock textile preforms. This model considered micro cells that were dividing the unit cell into a several structural regions. The fiber in the micro cells were assumed a series however the result of prediction showed less agreement with satin weave predictions.

Zhang and Harding used strain energy principle with finite element method for mechanical analysis of the textile composites [7]. In this model, the plain woven lamina was assumed having undulation in on direction and that is extended to 2D undulation model. A 2D crimp model is developed by Naik and Shebekar for elastic analysis of a 2D plain woven textile composites [8, 9]. This model was used extended 1D crimp model and incorporated the fiber undulation and continuity model to both of warp and weft yarns. The in-plane properties were

predicted with good agreement with experimental result in this model. Naik and Ganesh was developed two more models for analysis of woven textiles called as slice array model and element array model [10]. These models were discretized unit cell along the loading direction and elastic constants were estimated by assembling the elements of the unit cell. This model was also reported good agreement with experimental for prediction of mechanical properties of textile composite in plain weave model. Moreover, they were used these models to predict shear moduli and thermal properties of the laminate composites. After that, they developed 2D woven fabric composite strength model for 2D plain weave fabrics [11, 12]. Using this model, there were predicted the failure strength and stress behavior according to failure and strain history of uniaxial static loading condition and the effect of fabric geometry for the failure behavior.

A unit cell model for textile composite beams was proposed by Sanker and Marrey [13]. In this model, the material was assumed to be subjected to uniform state of strain. Hence, the displacement and traction was discontinuous between the faces of the unit cell. This method was verified with isotropic biomaterial beams and good agreement with experimental result both of beam and lamination theories. This method was used to evaluate the stiffness coefficients of composite beams with isotropic matrix. Ichihasi and his group developed numerical model with interfacial properties of woven fabrics [14]. In this model, between fiber bundles, a interphase element is inputted and the prediction showed that lower modulus and higher strength interface had a higher resistant to the micro fracture stress than on the interfacial strength.

Glaessgen and his group developed a method using the textile geometry model with finite element method for internal details of stress, strain, and failure

behavior of the composites [15]. In this method, a unit cell geometrical model is carried out to structural analysis of the composite. Cox developed ‘binary model’ for 3D textile composite in the elastic regime [16, 17]. In this model, axial properties of tows was represented by line element with two nodes. Based on these numerus analysis technics, to obtain accurate prediction of mechanical properties, there were more complex computational method is performed and developed [18, 19]. Whitcomb proposed a global-local finite element analysis method [18]. Coarse global model can be applied to obtain force and displacement and the value was used as boundary condition for local regions. This model had problems for probability of differences between stiffness of global and local models, however based on this model other numerical technics were developed [20]. Moreover, Woo and Whitcomb proposed 3D failure analysis of plain woven textile composites [21].

Chapman and Whitcomb investigated considering tow architecture model and in this model, a yarn was assumed having sinusoidal path and a lenticular cross section [22]. Whitcomb and Srirengan presented a model for simulating progressive failure model [23]. Also, progressive failure model is developed for laminated and woven composites [24]. A 3D finite element model developed by Dasgupta and Bhandarkar [25]. A homogenization study is used to predict the mechanical properties of composites. A self-consistent fabric geometry model was developed by Pastore and Gowayed. This mode was a modification of Fabric Geometry model [26] which is related the fiber architecture and stiffness averaging technics. An analytical model was proposed by Vandeurzen and in this model, a geometrical model of woven fabric structure is created [27]. This unit cell model was meshed micro cell and predicted local fiber volume fraction and yarn orientation. These developed model were implemented in a

custom software, TEXCOMP, however, the miss orientation of the yarn was neglected in the unit cell model. More 3D model of woven composites is researched for its mechanical properties [2, 27, 28]. Moreover, more application of fiber reinforced composites, 3D woven composite is developed and researched [29, 30].

In case of braided composites, it is also conventional structure and many numerical model existed. Finite element method has been applied to investigate the mechanical properties of braided composite. Ma proposed a diagonal brick model for braided textile composites [31]. This model was based on the simplified fiber unit cell structure as bulk resin with four yarn orientation diagonal bar element. The yarn orientation is assumed straight and crimping of fiber and interaction between yarns were ignored. Yang used lamination theory to predict elastic properties of 3D braided composites [32]. This model, called fiber inclination model, treated the unit cell of composites as an assemblage of inclined unidirectional laminate. This approach is extended of fiber undulation model, however verification test were not carried out although it was stated that the relevant prediction showed good agreement with experimental by other research. Braided composites is a 3D structure, two dimensional approach is researched [33].

It is also used in these days because of its fast computing time and feasible accuracy [34-37]. For example, Byun developed a geometric model using lamination analysis and stiffness averaging method [34]. In this model using 2D approximation of the classical lamination theory and variation in the braided yarn orientation is calculated in the unit cell model. This model had good agreement in axial tensile modulus, however, it showed a lack of shear modulus

prediction. A geometric model of 2D tri-axial braided textile composite was developed by Frank [38]. This model was used repeating unit cell for investigating effect of the architectural parameters on the mechanical properties of composites. For more analysis of mechanical behavior, unit cell modeling is used many times to numerically predict the elastic properties of 3D braided composites [39, 40]. Failure mechanism and strength is researched with unit cell modeling [1, 28, 41].

1.2.2 Failure criterion of FRPs

The failure criteria for FRPs has been studied numerous researchers over the last several decades [42-44]. Many types of approaches of FRPs failure analysis is done and demonstration of these failure criteria is still important issue in these days. Even though it is important progress, universally accepted failure criterion under general condition does not exist. According to a special edition of *Composites Science and Technology*, various failure theories of fibre reinforced plastic composites is used [45], and the survey performed by C.T. Sun on the industrial use of failure criteria [44, 46], Figure 2.

For laminates failure, it can be classified two types of criteria, one is associated with failure mode and the other is not. First, failure criteria that is not associated with failure modes are includes polynomial and tensorial criteria, using mathematical expressions to predict the failure surface as a function of the material strength. Generally, these expressions are based on the fundamental properties from experimental test. The most common polynomial failure criterion for composites is Tsai-Wu criterion [47]. This criterion is expressed in tensor notation as Eq. (1.1)

$$F_i \cdot \sigma_i + F_{ij} \cdot \sigma_i \cdot \sigma_j + F_{ijk} \cdot \sigma_i \cdot \sigma_j \cdot \sigma_k \geq 1 \qquad (1.1)$$

where i, j, k = 1, ... , 6 for a 3-D coordinate. The parameters F_i, F_{ij} and F_{ijk} are related to the lamina strengths in the principal directions. For using this criterion, due to the large number of material constants required, the third-order tensor F_{ijk} is usually neglected [48]. Therefore, the general polynomial criterion reduces to a general quadratic expression given by Eq. (1.2)

$$F_i \cdot \sigma_i + F_{ij} \cdot \sigma_i \cdot \sigma_j \geq 1 \tag{1.2}$$

Several other quadratic criteria also proposed, differing in the way in which the tensor stress components are determined. Tsai-Hill [49], Azzi-Tsai [50], Hoffman [51] and Chamis [52] are well-known quadratic failure criteria. These quadratic criteria can be represented in terms of the general Tsai-Wu criterion varying the parameters F_i and F_{ij}. These failure criteria are summarized in Table 1 [44]. These criteria do not take damage mechanisms and promote laminate failure. For using these criteria, homogenization is required for the lack of homogeneity govern the type of failure. Moreover, in these criteria, it is predicted that failure under biaxial tensile stresses depends on the compressive strength and it has physically problems.

Table 1. Polynomial Failure Criteria [44]

	Tasi-Wu	Tsai-Hill	Azzi-Tsai	Hoffman	Chamis
F_1	$\frac{1}{\sigma_{1T} - \sigma_{1C}}$	0	0	$\frac{1}{\sigma_{1T} - \sigma_{1C}}$	0

F_2	$\frac{1}{\sigma_{2T}-\sigma_{2C}}$	0	0	$\frac{1}{\sigma_{1T}-\sigma_{1C}}$	0
F_3	$\frac{1}{\sigma_{3T}-\sigma_{3C}}$	0	0	$\frac{1}{\sigma_{1T}-\sigma_{1C}}$	0
F_{12}	$\frac{-1}{2\sqrt{\sigma_{1T}\sigma_{1C}\sigma_{2T}\sigma_{2C}}}$	$-\frac{1}{2}\left(\frac{1}{\sigma_1^2}+\frac{1}{\sigma_2^2}-\frac{1}{\sigma_3^2}\right)$	$\frac{-1}{\sigma_1^2}$	$-\frac{1}{2}(T_1)$	$\frac{-K_{12}}{\sigma_1\cdot\sigma_2}$
F_{13}	$\frac{-1}{2\sqrt{\sigma_{1T}\sigma_{1C}\sigma_{3T}\sigma_{3C}}}$	$-\frac{1}{2}\left(\frac{1}{\sigma_3^2}+\frac{1}{\sigma_1^2}-\frac{1}{\sigma_2^2}\right)$	0	$-\frac{1}{2}(T_2)$	$\frac{-K_{13}}{\sigma_1\cdot\sigma_3}$
F_{23}	$\frac{-1}{2\sqrt{\sigma_{2T}\sigma_{2C}\sigma_{3T}\sigma_{3C}}}$	$-\frac{1}{2}\left(\frac{1}{\sigma_2^2}+\frac{1}{\sigma_3^2}-\frac{1}{\sigma_1^2}\right)$	0	$-\frac{1}{2}(T_3)$	$\frac{-K_{23}}{\sigma_2\cdot\sigma_3}$
F_{11}	$\frac{1}{\sigma_{1T}\cdot\sigma_{1C}}$	$\frac{1}{\sigma_1^2}$	$\frac{1}{\sigma_1^2}$	$\frac{1}{\sigma_{1T}\cdot\sigma_{1C}}$	$\frac{1}{\sigma_1^2}$
F_{22}	$\frac{1}{\sigma_{2T}\cdot\sigma_{2C}}$	$\frac{1}{\sigma_2^2}$	$\frac{1}{\sigma_2^2}$	$\frac{1}{\sigma_{2T}\cdot\sigma_{2C}}$	$\frac{1}{\sigma_2^2}$
F_{33}	$\frac{1}{\sigma_{3T}\cdot\sigma_{3C}}$	$\frac{1}{\sigma_3^2}$	0	$\frac{1}{\sigma_{3T}\cdot\sigma_{3C}}$	$\frac{1}{\sigma_3^2}$
F_{44}	$\frac{1}{\sigma_{23}^2}$	$\frac{1}{\sigma_{23}^2}$	0	$\frac{1}{\sigma_{23}^2}$	$\frac{1}{\sigma_{23}^2}$
F_{55}	$\frac{1}{\sigma_{13}^2}$	$\frac{1}{\sigma_{13}^2}$	0	$\frac{1}{\sigma_{13}^2}$	$\frac{1}{\sigma_{13}^2}$
F_{66}	$\frac{1}{\sigma_{12}^2}$	$\frac{1}{\sigma_{12}^2}$	$\frac{1}{\sigma_{12}^2}$	$\frac{1}{\sigma_{12}^2}$	$\frac{1}{\sigma_{12}^2}$

σ_i and σ_{ij} are normal and shear strength in each direction.

Subscript T is tension and C is compression.

K_{ij} is strength coefficient depending on the materials.

$$T_1=\left(\frac{1}{\sigma_{1T}\sigma_{1C}}+\frac{1}{\sigma_{2T}\sigma_{2C}}-\frac{1}{\sigma_{3T}\sigma_{3C}}\right),\ T_2=\left(\frac{1}{\sigma_{3T}\sigma_{3C}}+\frac{1}{\sigma_{1T}\sigma_{1C}}-\frac{1}{\sigma_{2T}\sigma_{2C}}\right),$$

$$\text{and } T_3=\left(\frac{1}{\sigma_{2T}\sigma_{2C}}+\frac{1}{\sigma_{3T}\sigma_{3C}}-\frac{1}{\sigma_{1T}\sigma_{1C}}\right),$$

The other types of failure criteria is associated with failure modes. These criteria is considered non-homogeneous structures and it is more suitable for composite characteristics. The criteria are established in terms of material strength and considered different failure of the constituents. These criteria have advantage of predicting failure mode and it is used for progressive failure analysis. For composite failure analysis, commonly three types of failure is considered mainly – fiber failure, transverse matrix failure, and shear matrix failure. Based on this, non-interactive failure criteria and interactive failure criteria can be classified. Non-interactive criteria does not take interactions between stress and strain on the composites. Typically, this is one of error point of strength predictions on multiaxial loading conditions and complex shape analysis. This type of failure criteria is maximum stress criterion and maximum strain criterion. Maximum stress criterion is considered composite failures that a failure occurs when the stress exceed the respective allowable. The failure condition is simple and direct way to predict failure and no interaction between the stresses acting on the composites considered. The failure condition is Eq. (1.3).

$$\begin{aligned} &Fiber \;-\; \sigma_1 \geq \sigma_{1T} \;\; or \;\; |\sigma_1| \geq \sigma_{1C} \\ &Matrix \;-\; \sigma_2 \geq \sigma_{2T} \;\; or \;\; |\sigma_2| \geq \sigma_{2C} \\ &Shear \;-\; |\sigma_{12}| \geq \sigma_{12} \end{aligned} \tag{1.3}$$

Maximum strain criterion is similar to maximum stress criterion. This criterion is considered the composite failure using ultimate failure strain. It is also simple and direct way to determine failure condition of the materials and considering

no interaction between strains on a composite. The failure condition is Eq. (1.4).

$$
\begin{aligned}
&Fiber \;\; - \;\; \varepsilon_1 \geq \varepsilon_{1T} \;\; or \;\; |\varepsilon_1| \geq \varepsilon_{1C} \\
&Matrix \;\; - \;\; \varepsilon_2 \geq \varepsilon_{2T} \;\; or \;\; |\varepsilon_2| \geq \varepsilon_{2C} \\
&Shear \;\; - \;\; |\varepsilon_{12}| \geq \varepsilon_{12}
\end{aligned}
\tag{1.4}
$$

Interactive failure criterion considers interaction between stress and strain that is acting on a composites. Hashin-Rotem [53] , Hashin [54], Puck [55] are well-known interactive failure criterion. Hashin-Rotem is considered tensile and compressive failure and distinguished these two types [53]. The failure condition is Eq (1.5)

$$
\begin{aligned}
&Fiber \;\; failure \\
&\sigma_1 = \sigma_{1T} \;\; (\sigma_1 > 0) \\
&-\sigma_1 = \sigma_{1C} \;\; (\sigma_1 < 0) \\
&Matrix \;\; failure \\
&\left(\frac{\sigma_2}{\sigma_{2T}}\right)^2 + \left(\frac{\sigma_{12}}{\sigma_{12u}}\right)^2 = 1 \;\; (\sigma_2 > 0) \\
&\left(\frac{\sigma_2}{\sigma_{2C}}\right)^2 + \left(\frac{\sigma_{12}}{\sigma_{12u}}\right)^2 = 1 \;\; (\sigma_2 < 0)
\end{aligned}
\tag{1.5}
$$

Hashin later proposed a failure criterion fir fiber reinforced composites under a 3D state of stress [54]. For the matrix failure, a linear criterion underestimates the material strength and high order polynomial criterion is complicated to deal with, so a quadratic approach was used. Moreover, the effect of shear stress is considered in the fiber failure mode. The failure condition is Eq (1.6)

Fiber failure

$$\left(\frac{\sigma_1}{\sigma_{1T}}\right)^2+\left(\frac{\sigma_{12}^2+\sigma_{13}^2}{\sigma_{12u}{}^2}\right)=1 \quad or\ \sigma_1=\sigma_{1T} \quad (\sigma_1>0)$$

$$-\sigma_1=\sigma_{1C} \quad (\sigma_1<0)$$

Matrix failure

$$\left(\frac{\sigma_2+\sigma_3}{\sigma_{2T}}\right)^2+\left(\frac{\sigma_{23}^2-\sigma_2\sigma_3}{\sigma_{23u}{}^2}\right)+\left(\frac{\sigma_{12}^2+\sigma_{13}^2}{\sigma_{12u}{}^2}\right)=1 \quad ((\sigma_2+\sigma_3)>0)$$

$$\left(\left(\frac{\sigma_{2C}}{2\sigma_{23u}}\right)^2-1\right)\left(\frac{\sigma_2+\sigma_3}{\sigma_{2C}}\right)+\left(\frac{\sigma_2+\sigma_3}{\sigma_{23u}{}^2}\right)^2$$

$$+\left(\frac{\sigma_{23}^2-\sigma_2\sigma_3}{\sigma_{23u}{}^2}\right)+\left(\frac{\sigma_{12}^2+\sigma_{13}^2}{\sigma_{12u}{}^2}\right)=1 \quad ((\sigma_2+\sigma_3)<0) \tag{1.6}$$

Puck was developed failure criterion considering two type of fracture condition [55]. One is fiber fracture and the other is inter fiber fracture. The particular difference of this criterion is considering three mode matrix failure that is inter fiber fracture. This algorithm explained more detail in the chapter 2 because this criterion used in this research.

Moreover, a number of authors have developed approaches for fiber and matrix failure which the different tension and compression properties. Yamada-Sun [56], Kroll-Hufenbach [57], Sun-Tao [46], Zinoviev [58], and Hart-Smith [48] is also widely used criterion for strength analysis of composites. Several representative interactive failure criterion summarized in Tables with classified by failure mode exclude already explained such as Hashin and Puck model. Table 2 is fiber tensile and compressive failure and Table 3 is matrix failure [59]. Also, fiber and matrix shear failure is considered many studies and it is summarized in Table 4

Table 2. Failure criteria for fiber failure [59]

Criterion	Type	Equation
Chang-Chang [24]	Tension	$\sqrt{\left(\frac{\sigma_1}{X_T}\right)^2 + \frac{\tau_{12}^2 / 2G_{12} + \frac{3}{4}\alpha\tau_{12}^4}{S_{12is}^2 / 2G_{12} + \frac{3}{4}\alpha S_{12is}^4}} \geq 1$ α from non-linear shear law
Chang-Lessard [60]	Compre-ssion	$\sigma_1 \geq \bar{X}_c$ (microbuckling strength)
LaRC04 [61]	Compre-ssion	$For\ \sigma_{2m2m} < 0,\ \frac{\lvert\tau_{1m2m}\rvert}{S_{12is} - \eta_{12}\sigma_{2m2m}} \geq 1$ $For\ \sigma_{2m2m} < 0,\ (1-g)\left(\frac{\sigma_{2m2m}}{Y_{Tis}}\right)$ $+g\left(\frac{\sigma_{2m2m}}{Y_{Tis}}\right)^2 + \frac{\Lambda_{23}^0\tau_{2m3\varphi}^2 + \chi(\gamma_{1m2m})}{\chi(\gamma_{12is}^u)} \geq 1$ Stresses are in 3D kinking frame at angle ψ and g=G_{Ic}/G_{IIc} difference for thin and thick plies
Maimi [62]	Compre-ssion	$\left\langle \lvert\tau_{12}^m\rvert + \eta_{12}\sigma_{22}^m \right\rangle / S_{12} \geq 1$ Stresses are in 2D kinking frame
Lee [63]	Mixed	$\sigma_1 \geq \sigma_{FN}\ or\ \sqrt{\sigma_{12}^2 + \sigma_{13}^2} \geq \sigma_{FS}$ FN is fiber normal strengthand FS is fiber in-plane shear strength

Christensen [64]	Mixed	$\alpha_2 k_2 \sigma_1 + \frac{1}{4}(1+2\alpha_2)\sigma_1^2 - \frac{(1+2\alpha_2)^2}{2}\frac{(\sigma_2+\sigma_3)}{2}\sigma_1 \geq k_2^2$ $k_2 = \frac{X_T}{2}, \alpha_2 = \left(\frac{X_T}{\lvert X_c \rvert}\right) - 1$

Table 3. Failure criteria for matric failure [59]

Criterion	Type	Equation
Chang-Chang [24]	Tension	$\sqrt{\left(\frac{\sigma_2}{Y_T}\right)^2 + \frac{\tau_{12}^2 / 2G_{12} + \frac{3}{4}\alpha\tau_{12}^4}{S_{12is}^2 / 2G_{12} + \frac{3}{4}\alpha S_{12is}^4}} \geq 1$ α from non-linear shear law
Shahid-Chang [65]	Tension	$\left(\frac{\bar{\sigma}_2}{Y_T(\phi)}\right)^2 + \left(\frac{\bar{\tau}_{12}}{S_{12}(\phi)}\right)^2 \geq 1$ Stresses are effective stress and φ is matrix crack density
LaRC04 [61]	Tension	$(1-g)\left(\frac{\sigma_2}{Y_{Tis}}\right) + g\left(\frac{\sigma_2}{Y_{Tis}}\right)^2 + \frac{\Lambda_{23}^0 \tau_{23}^2 + \chi(\gamma_{12})}{\chi(\gamma_{12is}^u)} \geq 1$ $g = G_{Ic}/G_{IIc}$

Maimi [62]	Tension	$For\ \sigma_2 \geq 0,\ \sqrt{(1-g)\left(\frac{\sigma_2}{Y_T}\right) + g\left(\frac{\sigma_2}{Y_T}\right)^2 + \left(\frac{\tau_{12}}{S_{12}}\right)^2} \geq 1$ $For\ \sigma_2 < 0,\ \left\langle \lvert\tau_{12}\rvert + \eta_{12}\sigma_2 \right\rangle / S_{12} \geq 1$
LaRC04 [61]	Compre-ssion	$For\ \sigma_1 \geq -Y_c,$ $\left(\frac{\tau_{23}^{\alpha}}{S_{23} - \eta_{23}\sigma_n}\right)^2 + \left(\frac{\tau_{12}^{\alpha}}{S_{12is} - \eta_{12}\sigma_n}\right)^2 \geq 1$ $For\ \sigma_1 < -Y_c,$ $\left(\frac{\tau_{23}^{m}}{S_{23} - \eta_{23}\sigma_n^m}\right)^2 + \left(\frac{\tau m}{S_{12is} - \eta_{12}\sigma_n^m}\right)^2 \geq 1$
Maimi [62]	Compre-ssion	$\sqrt{\left(\frac{\tau_{23eff}}{S_{23}}\right)^2 + \left(\frac{\tau_{12eff}}{S_{12}}\right)^2} \geq 1$ $\tau_{23eff} = \left\langle -\sigma_{22}\cos\alpha_0(\sin\alpha_0 - \eta_{23}\cos\alpha_0\cos\theta) \right\rangle$ $\tau_{12eff} = \left\langle \cos\alpha_0(\lvert\tau_{12}\rvert - \eta_{23}\sigma_{22}\cos\alpha_0\sin\theta) \right\rangle$ $\alpha_0 = 53^{\circ}$
Lee [63]	Mixed	$\sigma_2 \geq \sigma_{MN}\ or\ \sqrt{\sigma_{12}^2 + \sigma_{13}^2} \geq \sigma_{MS}$ MN is matrix normal strength and MS is matrix shear strength
Christensen [64]	Mixed	$\alpha_1 k_1(\sigma_2 + \sigma_3) + (\sigma_{12}^2 + \sigma_{31}^2) +$ $(1 + 2\alpha_1)\left[\frac{1}{4}(\sigma_2 - \sigma_3)^2 + \sigma_{23}^2\right] \geq k_1^2$ $k_1 = S_{12} = \frac{1}{2}\lvert Y_c\rvert,\ \alpha_1 = \frac{1}{2}\left(\lvert Y_c\rvert / Y_T - 1\right)$

Table 4. Failure criteria for fiber-matrix shear failure [59]

Criterion	Equation
Chang-Lessard [60]	$\sqrt{\left(\frac{\sigma_1}{X_C}\right)^2 + \frac{\tau_{12}^2 / 2G_{12} + \frac{3}{4}\alpha\tau_{12}^4}{S_{12is}^2 / 2G_{12} + \frac{3}{4}\alpha S_{12is}^4}} \geq 1$ α from non-linear shear law
Ladeveze [66]	*Use* $d_{12}, \bar{\psi}_{12}, \bar{\psi}_2$ *to indicate damage* *total failure for* $d_{12} \geq 1$ *or* $\bar{\psi}_2 \geq \psi_{2\max}$ $d_{1,12} = \langle \bar{\psi}_{1,12} - \psi_{1,12crit} \rangle_+ / \psi_{1,12crit}$ $\bar{\psi}_{12}(t) = \sqrt{\tau_{12}^2 / (2G_{12}(1-d_{12})^2)} + b\bar{\psi}_2(t)$ $\bar{\psi}_2(t) = \sqrt{\frac{1}{2}\frac{\langle \sigma_2 \rangle_+^2}{E_2(1-d_2)}}$, $\bar{\psi}_{12} = \max \bar{\psi}_{12}(t)$ *based on tensile coupon test*
Shahid-Chang [65]	$\left(\frac{\bar{\sigma}_1}{X_T}\right)^2 + \left(\frac{\bar{\tau}_{12}}{S_{12}(\phi)}\right)^2 \geq 1$ Stresses are effective stress and φ is matrix crack density

Using these failure criterion that is described deal with a lamina, a laminate strength prediction is processed. The progressive damage leads to final failure so laminate failure is complicated than unidirectional lamina composite analysis. Moreover, in the laminates, more damage mechanism occurs such as delamination and interaction of lamina. A number of criteria have been proposed to predict the delamination of composites. The initiation of

delamination is investigated many works and they are summarized in Table 5 and these criteria use combination of the through thickness tensile and shear parameters. Wisnom et al. [67] was a particular approach for this that is using principle stresses. Moreover, criteria for predicting the growth of an existing delamination and almost these criteria are based on the fracture mechanics concept of a strain release rate [59]. Due to the complex phenomena of laminated composites, the onset of damage does not usually lead to ultimate failure so damage modeling and mechanics is required for composite strength analysis and it is necessary to account for the loss of performance cause by damage. Damage propagation is important for accurate prediction of composite material properties. It is surely that numerous models have been developed for damage mechanisms and these damage model have been used both in conjunction with and independent of the failure criteria for damage initiation. A common approach of damage model is applying both in-plane and inter-laminar damage. A comprehensive review of damage mechanics theories is given by Talreja [68].

Table 5. Failure criteria for delamination initiation [59]

Criterion	Equation
Max stress	$\sigma_3 \geq Z_T, \tau_{31} \geq S_{31}, \tau_{23} \geq S_{23}$
Hashin [54]	$\left(\frac{\sigma_3}{Z_T}\right)^2 + \left(\frac{\tau_{23}}{S_{23}}\right)^2 + \left(\frac{\tau_{31}}{S_{31}}\right)^2 \geq 1$
Lee [63]	$\sigma_3 \geq Z_T \ or \ \sqrt{(\sigma_{12}^2 + \sigma_{13}^2} \geq S_{23}$
Ochoa-Engblom [69]	$\left(\frac{\sigma_3}{Z_T}\right)^2 + \left(\frac{\tau_{23}^2 + \tau_{31}^2}{S_{23}^2}\right) \geq 1$

Brewer-Lagace [70]	$\left(\frac{\tau_{23}}{S_{23}}\right)^2+\left(\frac{\tau_{31}}{S_{31}}\right)^2+\left(\frac{\sigma_3^+}{Z_T}\right)^2+\left(\frac{\sigma_3^-}{Z_C}\right)^2\geq 1$
Degen-Tsai [71]	$\left(\frac{\sigma_1}{X_T}\right)^2+\left(\frac{\sigma_3}{Z_T}\right)^2+\left(\frac{\tau_{23}}{S_{23}}\right)^2\geq 1$
Tong-Norris [71]	$\left(\frac{\sigma_1^2-\sigma_1\sigma_3}{X_T X_C}\right)+\left(\frac{\sigma_3}{Z_T}\right)+\left(\frac{\tau_{23}}{S_{23}}\right)^2\geq 1$
Zang [72]	$\sigma_3\geq Z_T \ and \ \sqrt{(\tau_{31}^2+\tau_{23}^2}\geq S_{23}$
Wisnom [67]	Effective matrix stress σ_e found from principal stresses $2.6\sigma_e^2=(\sigma_1-\sigma_2)^2+(\sigma_2-\sigma_3)^2+(\sigma_3-\sigma_1)^2$ $+0.6\sigma_e(\sigma_1+\sigma_2+\sigma_3)$
Goyal [73]	$\left(\frac{\tau_{23}}{S_{23}}\right)^\gamma+\left(\frac{\tau_{31}}{S_{31}}\right)^\gamma+\left(\frac{\sigma_3^+}{Z_T}\right)^2\geq 1$ γ is curve fit parameter

1.3 Research objectives

Previous numerical models are well developed and established technology for given structure and system of fiber reinforced composites. However, nevertheless many numerical model of fiber reinforced composites existed, there is still studying in many parts of various structure and manufacturing because the composites has lots of parameters those influence to mechanical properties and significant differences each composite systems. So almost research have focused on a specific system of composites

For this reason, in this study, we developed a new numerical approach to analysis mechanical properties of fiber reinforced composites. The aim of new method is universal usage for any structure composites and structural analysis using minimum input parameters and experimental data with feasible accuracy. For this purpose, we focused on inner fiber structure of composites. First, we considered the yarn orientation according to unit cell approach because it is most important factor to mechanical behavior of the composites. A yarn orientation update algorithm was developed with deformation gradient to reflect the change of them. Using this yarn orientation, the inner structure of the composite was defined. The elastic property of the composite was calculated using layer model based on the mechanical properties of the unidirectional composites and yarn orientation. Partial damage and propagation was also considered for analyzing the failure behavior of the braided composite. The partial failure conditions were obtained by unidirectional composites and tensor transform then used in damage analysis. The failure condition was formulated using three-dimensional Puck's criterion. The numerical analysis was carried out using ABAQUS, the results of which were compared with experimental results for the validation purpose.

Chapter 2. Fiber based continuum model (FBM)

2.1 Fiber based analysis mechanism

In this study, we developed a new numerical approach to analysis mechanical properties of fiber reinforced composites especially 3D textile composites. New method is focused on multiscale analysis with inner fiber structure of the composites because of continuum level approach of 3D textile composites. Moreover, based on continuum model, including mesoscale analysis, there is needed that feasible accuracy and computing cost with one step finite element analysis. For this purpose, we developed new numerical analysis model, called fiber based continuum model (FBM) that focused on inner fiber orientation of composites. First, we considered the yarn orientation because it is most important factor to mechanical behavior of the composites. A yarn orientation update algorithm was developed with deformation gradient. Using this updated yarn orientation, the inner structure of the composite was defined. The elastic property of the composite was calculated based on the mechanical properties of the material properties, tensor transform, and yarn orientation. Failure analysis was done with partial damage and propagation. The partial failure conditions were obtained by unidirectional composites and tensor transform then used in damage analysis. The failure condition was formulated using three-dimensional Puck's criterion. The numerical analysis was carried out using commercial finite element analysis software, ABAQUS.

In this chapter, FBM is explained with step-by-step as four sequence. Here, the modulus, strength, and damage mode and propagation of composites can be obtained with this FBM analysis.

2.2 Numerical approach

2.2.1 Methodology of mechanical prediction of FRPs

A new numerical analysis method was developed that can reflect the microstructural change of the textile structure and can calculate the stress increments due to the deformation. The schematic diagram of new model as shown Figure 2-1.

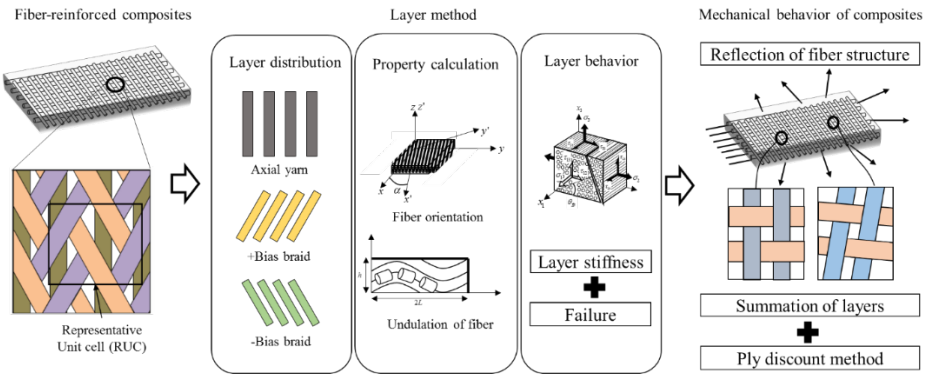

Figure 2-1. Schematic diagram of fiber based analysis model

Fiber structure is most important parameter in composite properties, so for reflecting this fiber structure and universal approach of fiber reinforced composites, we were done sectioning of composites' inner structure. For this, we used layer method for stiffness and strength prediction of composites form other previous researches [35, 37]. There were focused stiffness and 2D approximation of 3D braided composites, however in this research, we use this layer method for both of stiffness and strength analysis. This model is based on

continuum approach and assumed perfect inner structure with no interfacial effect and simple assumption of fiber location. Also we assumed linear elastic properties in this study. So, numerical error of this method would be larger than 3D unit cell modeling. However, even though this method cannot reflect these effect, this approach predict composite properties using just a unidirectional layer properties. This method has advantage for fiber reinforced composites design due to very fast computing cost and simple calculation step for complex structure of composites. Moreover, for more accuracy of the prediction and mimicking stress-strain behavior, we adopt modified ply discount method in this fiber based analysis model. This new model consist of four steps as shown Figure 2-2.

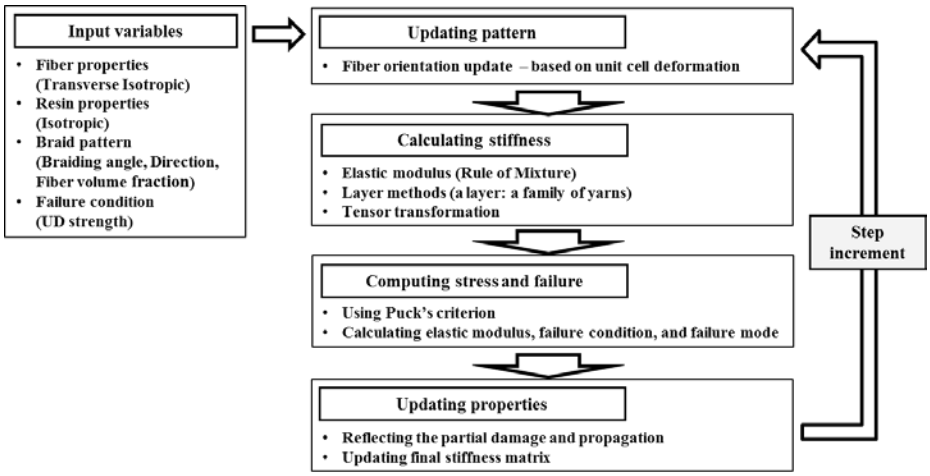

Figure 2-2. Four step flow chart of fiber based analysis model

2.2.2 Algorithm of update yarn pattern

First step is yarn orientation definition. The orientation of yarn is defined using

direction cosine. This orientation is updated each increment step using deformation gradient. Here, the orientation is calculated based on unit cell deformation and we assumed internal unit cell structure is not changed such as internal yarn undulation and internal delamination. Figure 2-3 is schematic diagram of yarn deformation and its update. P` vector is deformed vector from P vector and the deformation calculation is according to deformation gradient as Eq. (2.1).

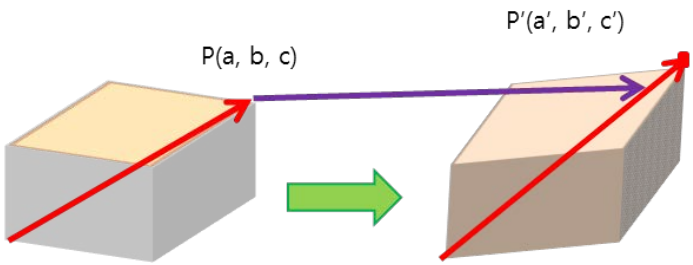

Figure 2-3. Schematic diagram of yarn vector deformation

$$[DFG] = \begin{bmatrix} F_{11} & F_{12} & F_{13} \\ F_{21} & F_{22} & F_{23} \\ F_{31} & F_{32} & F_{33} \end{bmatrix} \qquad (2.1)$$
$$\{P'\} = [F]\{P\}$$

2.2.3 Stiffness calculation of FRPs

Based on the yarn orientation, the yarn angle was updated each section for computing the stiffness matrix of unit cell. 3D tangent stiffness matrix of the composites was calculated for their elastic behavior considering yarn

orientation. For unit cell stiffness matrix, we use tensor calculations based on layer-by- layer approach that was mentioned before [35, 37]. This model is based on 2D approach with tensor transform, however, in this research 3D yarn path is considered for universal fiber structure investigation. Here is the sequence of the stiffness calculation. To calculate the stiffness matrix of unit cell, the unit cell is consist of several parts of composite layers and total properties is supposed to composed of these composite layers. Each composite layer, mechanical properties is calculated using the rule of mixture as Eq. (2.2).

$$
\begin{aligned}
&V_m = 1 - V_f \\
&E_{11} = E_{11f} \times V_f + V_m \times E_m \\
&E_{22} = 1/((V_f / E_{22f}) + (V_m / E_m)) \\
&\nu_{12} = \nu_{12f} \times V_f + \nu_m \times V_m \\
&\nu_{23} = \nu_{12}(1 - \nu_{12} \times (E_{22} / E_{11})) / (1 - \nu_{12}) \\
&G_{12} = G_{12f} \times G_m / (G_{12f} \times \nu_m) + (G_m \times \nu_f)) \\
&G_{23} = E_{22} / (2 \times (1 + \nu_{23}))
\end{aligned}
\tag{2.2}
$$

where E and G are the Young's and shear modulus. V is volume fraction and subscript f is fiber and m is matrix. v is Poisson's ratio. Here, each composite layer is assumed having transverse isotropic properties and the stiffness matrix can be represented as Eq. (2.3) [35].

$$
\begin{aligned}
&C_{11} = (1 - v_{23}^2)\frac{E_{11}}{V}, \quad C_{12} = C_{13} = v_{12}(1 - v_{23})\frac{E_{22}}{V} \\
&C_{23} = (v_{23} + v_{12}^2 \frac{E_{22}}{E_{11}})\frac{E_{22}}{V}, \quad C_{22} = C_{33} = (1 - v_{12}^2 \frac{E_{22}}{E_{11}})\frac{E_{22}}{V}, \\
&C_{44} = G_{23} = \frac{E_{22}}{2(1 + v_{23})}, \quad C_{55} = C_{66} = G_{12} \\
&where \;\; V = \left[(1 + v_{23})\left(1 - v_{23} - 2v_{12}^2 \frac{E_{22}}{E_{11}} \right) \right]
\end{aligned}
\tag{2.3}
$$

C_{ij} is each component of stiffness matrix at each direction. Here, another composite analytical model is accepted for the yarn undulation as tow crimp effect. For this, as Figure 2-4, inner yarn undulation is considered as a sinusoidal function like Eq. (2.4) [35]. A is thickness of a unit cell and 2L is a wave length of sinusoidal fiber. In this study, we use initial unit cell dimension is used for this parameter and it is measured form experimental samples. Based on this yarn undulation, the averaged layer stiffness is calculated over one wavelength with Eq. (2.5)-(2.7). Eq. (2.5) and (2.6) is transform matrix for the undulation and (2.7) is summation for each layer stiffness.

$$
\begin{aligned}
&z' = A\sin\left(\frac{\pi x'}{L}\right), \quad \tan(\beta) = \frac{\pi A}{L}\cos\left(\frac{\pi x'}{L}\right) \\
&\hat{m} = \cos(\beta) = \frac{1}{\sqrt{1 + \tan^2(\beta)}}, \quad \hat{n} = \sin(\beta) = \frac{\tan(\beta)}{\sqrt{1 + \tan^2(\beta)}}
\end{aligned}
\tag{2.4}
$$

$$\hat{T}_1 = \begin{bmatrix} \hat{m}^2 & 0 & \hat{n}^2 & 0 & 2\hat{m}\hat{n} & 0 \\ 0 & 1 & 0 & 0 & 0 & 0 \\ \hat{n}^2 & 0 & \hat{m}^2 & 0 & -2\hat{m}\hat{n} & 0 \\ 0 & 0 & 0 & \hat{m} & 0 & -\hat{n} \\ -\hat{m}\hat{n} & 0 & \hat{m}\hat{n} & 0 & \hat{m}^2 - \hat{n}^2 & 0 \\ 0 & 0 & 0 & \hat{n} & 0 & \hat{m} \end{bmatrix} \tag{2.5}$$

$$\hat{T}_2 = \begin{bmatrix} \hat{m}^2 & 0 & \hat{n}^2 & 0 & \hat{m}\hat{n} & 0 \\ 0 & 1 & 0 & 0 & 0 & 0 \\ \hat{n}^2 & 0 & \hat{m}^2 & 0 & -\hat{m}\hat{n} & 0 \\ 0 & 0 & 0 & \hat{m} & 0 & -\hat{n} \\ -2\hat{m}\hat{n} & 0 & 2\hat{m}\hat{n} & 0 & \hat{m}^2 - \hat{n}^2 & 0 \\ 0 & 0 & 0 & \hat{n} & 0 & \hat{m} \end{bmatrix} \tag{2.6}$$

$$\begin{aligned} \{\sigma\} &= \frac{1}{2l}\int_0^{2l} \left[\hat{T}_1\right]^{-1} [C] \left[\hat{T}_2\right] dx \{\varepsilon\} \\ \{\sigma\} &= \left[\bar{C}\right]\{\varepsilon\} \end{aligned} \tag{2.7}$$

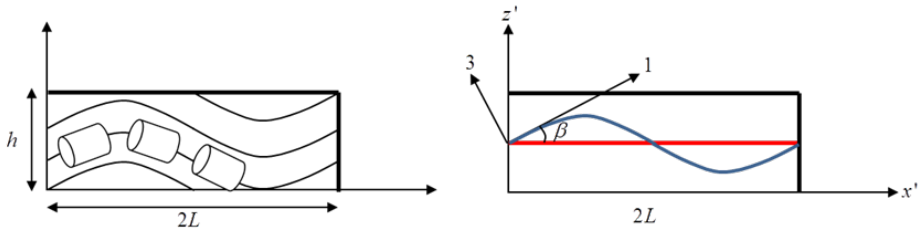

Figure 2-4. Yarn undulation for braided composites of fiber based analysis model

Next step is a tow rotation calculation about the z-axis. Figure 2-5 is rotation coordinate according to yarn angle. For braided composites, the angel is braiding angle. Eq. (2.8) and (2.9) are rotation matrices about tow rotation and Eq. (2.10) is stiffness tensor transform calculation. In this calculation, compliance matrix is used for off axis yarn due to compliance matrix has more accuracy on matrix rich region. So one more algorithm is added as Figure 2-6. Off axis layer calculation is used this compliance matrix form. Eq. (2.11) is tensor transform for compliance matrix. Briefly, on axis layer is used tensor transform as Eq. (2.10) and off axis layer is used as Eq. (2.11). After transform calculation, compliance matrix is changed to stiffness matrix for next step. On and off axis is defined with loading direction. The differences of two method is discussed at section 2.3.

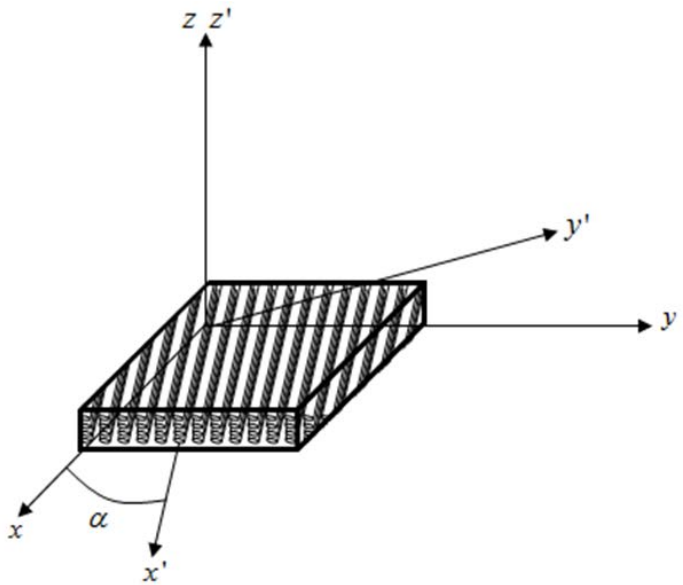

Figure 2-5. Rotation coordinate according to yarn angle in the composite

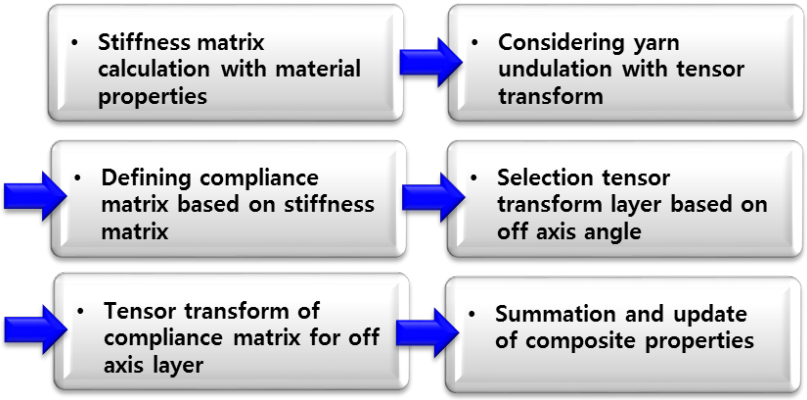

Figure 2-6. Flowchart of compliance matrix calculation for off axis layer

$$T_1 = \begin{bmatrix} m^2 & n^2 & 0 & 0 & 0 & 2mn \\ n^2 & m^2 & 0 & 0 & 0 & -2mn \\ 0 & 0 & 1 & 0 & 0 & 0 \\ 0 & 0 & 0 & m & -n & 0 \\ 0 & 0 & 0 & n & m & 0 \\ -mn & mn & 0 & 0 & 0 & m^2 - n^2 \end{bmatrix} \tag{2.8}$$

$$T_2 = \begin{bmatrix} m^2 & n^2 & 0 & 0 & 0 & mn \\ n^2 & m^2 & 0 & 0 & 0 & -mn \\ 0 & 0 & 1 & 0 & 0 & 0 \\ 0 & 0 & 0 & m & -n & 0 \\ 0 & 0 & 0 & n & m & 0 \\ -2mn & 2mn & 0 & 0 & 0 & m^2 - n^2 \end{bmatrix} \tag{2.9}$$

$$\{\sigma\} = [T_1]^{-1}\left[\overline{C}\right][T_2]\{\varepsilon\} \tag{2.10}$$

$$\begin{aligned}
&[S] = [C]^{-1} \\
&\left[\overline{C}\right] = [T_1]^{-1}[C][T_2] \\
&\left[\overline{S}\right] = \left[\overline{C}\right]^{-1} = \left([T_1]^{-1}[C][T_2]\right)^{-1} = [T_2]^{-1}[S][T_1]
\end{aligned} \tag{2.11}$$

where m is cos(α) as tow rotation angle and n is sin(α).

Here, we was done one more transform steps for 3D approximation of the fiber structure according to thickness, using Eq. (2.5) and (2.6). After that, a composite stiffness is determined summation of each yarn part stiffness matrix as Eq. (2.12)

$$[C^{RUC}] = h^{+a}\left[C_{global}\right]^{+a} + h^{-a}\left[C_{global}\right]^{-a} + h^{0}\left[C_{global}\right]^{0} \tag{2.12}$$

2.2.4 Strength prediction and damage propagation

Based on above steps, unit cell stiffness matrix is defined. Also, using this matrix, elastic properties was calculated. Next sequence is detection of partial damage and propagation. They were incorporated into the stress calculation using partial damage and failure with ply discount method. Here, we also use layer method for partial damage detection. Each layer failure condition is defined using Puck's criterion as Figure 2-7 and Eq. (2.13) and (2.14) [55, 74]. Eq. (2.13) is fiber failure mode under tensile and compressive stress and Eq. (2.14) is inter fiber failure mode.

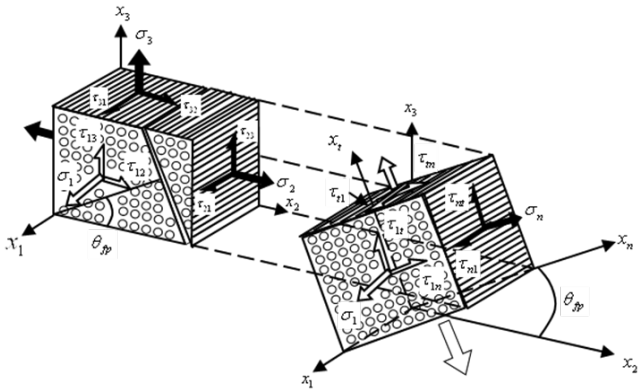
x_3
σ_3
τ_{31}
τ_{32}
τ_{13}
τ_{12}
σ_1
τ_{21}
σ_2
x_2
x_1
θ_{fp}
x_3
x_t
τ_m
τ_{n1}
τ_{nt}
σ_n
τ_{1t}
τ_{n1}
τ_{1n}
σ_1
x_n
θ_{fp}
x_2
x_1

(a)

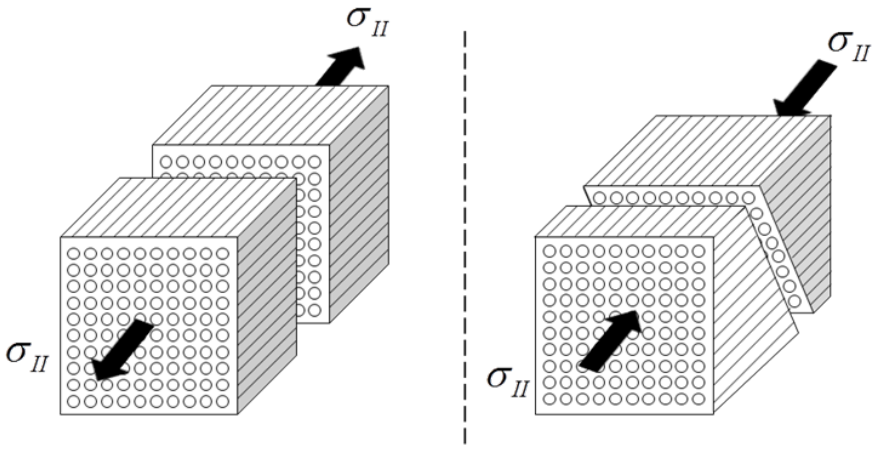
σ_{II}
σ_{II}
σ_{II}
σ_{II}

(b)

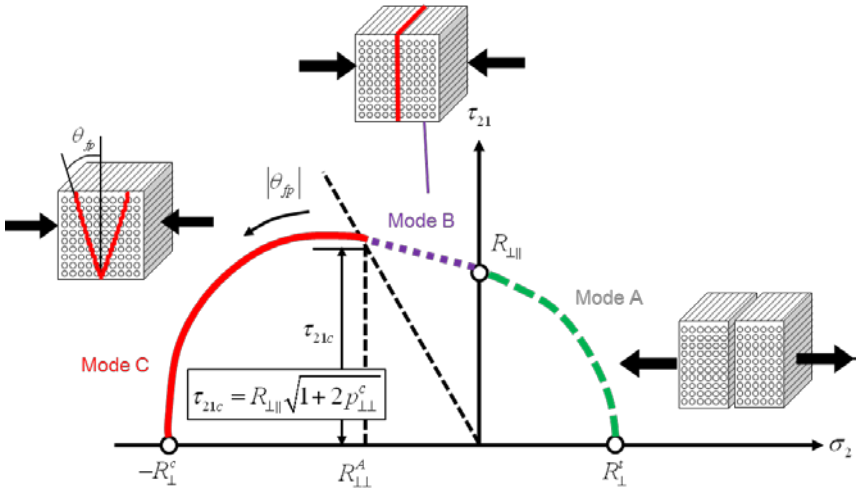

(c)

Figure 2-7. . Puck's failure criterion (a) tensor transform for 3D stress, (b) fiber failure mode of tension (left) and compression (right), (c) inter fiber failure mode according to stress distribution

$$\frac{1}{\varepsilon_{1T}}\left(\varepsilon_1 - \frac{\nu_{f12}}{E_{f1}} m_{\sigma f}\sigma_2\right) = 1$$
$$\frac{1}{\varepsilon_{1C}}\left|\left(\varepsilon_1 - \frac{\nu_{f12}}{E_{f1}} m_{\sigma f}\sigma_2\right)\right| = 1 - \left(10\gamma_{21}\right)^2 \tag{2.13}$$

For $\sigma_n(\theta) \geq 0$:

$$f_E(\theta) = \sqrt{\left[\left(\frac{1}{R_{\perp}^{(+)A}} - \frac{p_{\perp\psi}^{(+)}}{R_{\perp\psi}^{A}}\right)\sigma_n(\theta)\right]^2 + \left(\frac{\tau_{nt}(\theta)}{R_{\perp\perp}^{A}}\right)^2 + \left(\frac{\tau_{nl}(\theta)}{R_{\perp\parallel}^{A}}\right)^2} + \frac{p_{\perp\psi}^{(+)}}{R_{\perp\psi}^{A}}\sigma_n(\theta)$$

For $\sigma_n(\theta) < 0$:

$$f_E(\theta) = \sqrt{\left(\frac{\tau_{nt}(\theta)}{R_{\perp\perp}^{A}}\right)^2 + \left(\frac{\tau_{nl}(\theta)}{R_{\perp\parallel}^{A}}\right)^2 + \left[\frac{p_{\perp\psi}^{(-)}}{R_{\perp\psi}^{A}}\sigma_n(\theta)\right]^2} + \frac{p_{\perp\psi}^{(-)}}{R_{\perp\psi}^{A}}\sigma_n(\theta)$$

where

$$\frac{p_{\perp\psi}^{(+)}}{R_{\perp\psi}^{A}} = \frac{p_{\perp\perp}^{(+)}}{R_{\perp\perp}^{A}}\cos^2\psi + \frac{p_{\perp\parallel}^{(+)}}{R_{\perp\parallel}^{A}}\sin^2\psi \qquad \cos^2\psi = \frac{\tau_{nt}^2}{\tau_{nt}^2 + \tau_{nl}^2}$$

$$\frac{p_{\perp\psi}^{(-)}}{R_{\perp\psi}^{A}} = \frac{p_{\perp\perp}^{(-)}}{R_{\perp\perp}^{A}}\cos^2\psi + \frac{p_{\perp\parallel}^{(-)}}{R_{\perp\parallel}^{A}}\sin^2\psi \qquad \sin^2\psi = \frac{\tau_{nl}^2}{\tau_{nt}^2 + \tau_{nl}^2}$$

$$R_{\perp}^{(+)A} = Y_T; \quad R_{\perp\parallel}^{A} = S_{21}; \quad R_{\perp\perp}^{A} = \frac{Y_c}{2\left(1 + p_{\perp\perp}^{(-)}\right)} \tag{2.14}$$

The factor $m_{\sigma f}$ is a mean magnification factor and the value is used in this study 1.3 for glass fiber and 1.1 for carbon fiber according to Puck's theory [55]. Finally, the stiffness matrix was updated including partial damage failure for next increment. The algorithm developed above was implemented into ABAQUS for numerical analysis, for which a UMAT subroutine was developed. In the UMAT, we use state variable for tracing partial damage and propagation.

2.2.5 Stress update and processing increment

Finial step is damage propagation and stress update step. Calculating an increment stress and strain behavior is defined and update in this step. Failure layer properties are degraded based on ply discount model as Table 6 [75-77].

Here we used a modified ply discount model that was not a total stiffness degradation and specific direction material properties were degradation. Because, in case of using a large failure strain resin, even fiber failure occur inside composite, stress is sustained by a resin and interfacial load transfer. Also numerical stability we use 10^{-5} value instead of 0 for modulus and Poisson's ratio.

Table 6. Material degradation rule based on ply discount model

Failure modes	Failure condition	Degradation properties (f=fiber, m=matrix)
Fiber tensile failure	$\sigma_{11} > 0$	$E_{f11} = 0$, $v_{f12} = 0$, $G_{f12} = 0$
Fiber compressive failure	$\sigma_{11} < 0$	
Matrix tensile failure	$\sigma_{22} > 0$ / $\sigma_{33} > 0$	$E_{f22} = 0$, $G_{f12} = 0$, $E_m = 0$, $v_m = 0$, $G_m = 0$
Matrix compression failure	$\sigma_{22} > 0$ / $\sigma_{33} > 0$	

σ_i and σ_{ij} are normal and shear strength in each direction.

2.3 Characterization and validation of the model

2.3.1 Model characterization

At first, the effect of FBM model, 2D numerical model is compared to FBM analysis. Figure 2-8 is moduli comparison between reference 2D model and

FBM. As figure 2-8(a) X and Y direction modulus is not much difference due to FBM model is also fundamentally based reference undulation model. However, as Figure 2-8(b), Z direction modulus shows large difference between reference and FBM. Reference model is 2D approximation model, so not focused and considered Z direction properties. FBM is focused on 3D structural analysis so focused on Z-direction effect together with tensor calculation. Its effect is also shown shear modulus and Poisson's ratio. Figure 2-8(c) and (d) shows the difference of two models numerical results.

Compliance matrix calculation is explained at section 2.2.3 and it has advantage for 3D textile composite mechanical properties prediction. Figure 2-9 shows an example of differences that the modulus between stiffness calculation and compliance calculation. Figure 2-9 is a five-axis braided composite example with carbon fiber and 45 % fiber volume fraction. XY plane properties is almost same between two calculation methods, however there is huge difference at thickness direction modulus. This model based on layer method, so thickness direction modulus is same even XY plane yarn angle is changed. Stiffness calculation model has changing according to braiding angle and it is numerical error. In case of compliance form calculation, it has also change, however it is small value that can be neglect.

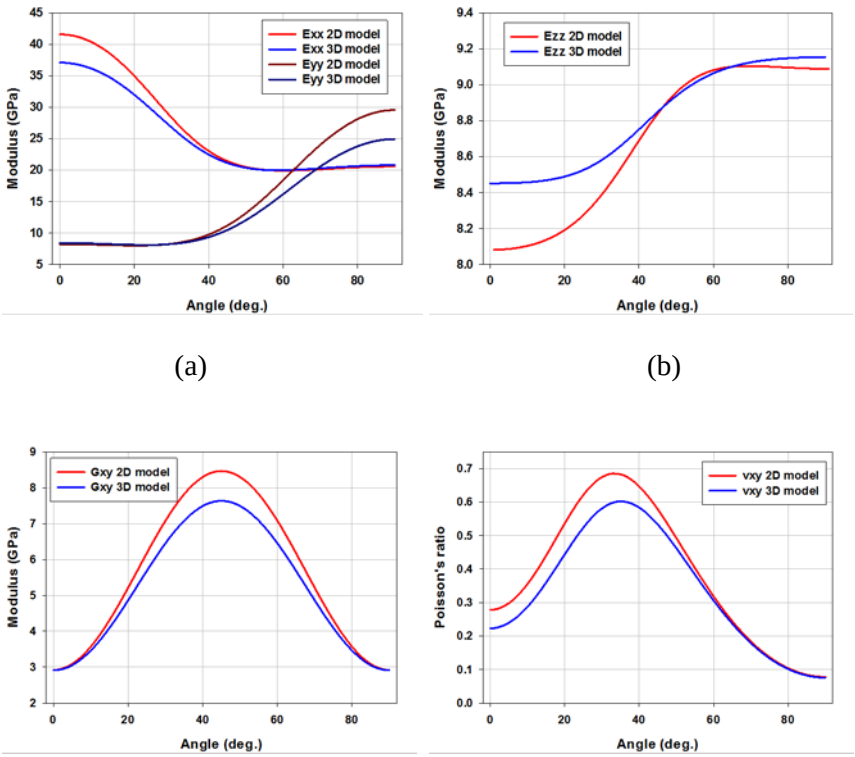

(a) (b)

(c) (d)

Figure 2-8. Numerical analysis result of 3D braided composite moduli using two types of prediction model according to braided angle. (a) X and Y direction tensile modulus comparison, (b) Z direction tensile modulus, (c) shear modulus of XY direction and (d) Poisson's ratio of XY direction

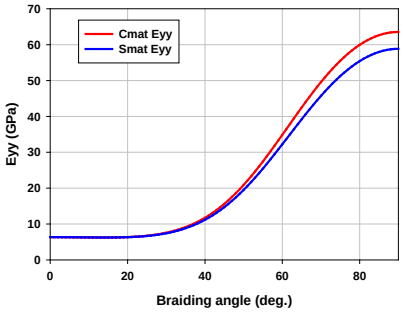
Cmat Eyy
Smat Eyy
Eyy (GPa)
Braiding angle (deg.)

(a)

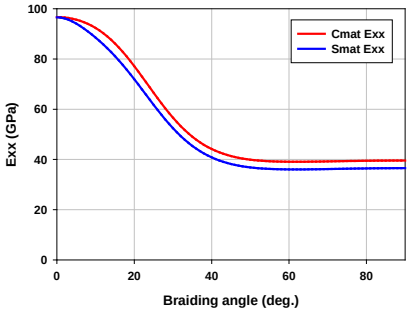
Cmat Exx
Smat Exx
Exx (GPa)
Braiding angle (deg.)

(b)

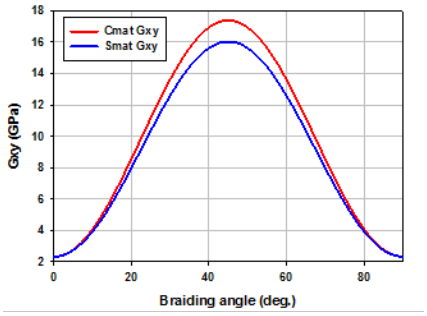
Cmat Gxy
Smat Gxy
Gxy (GPa)
Braiding angle (deg.)

(c)

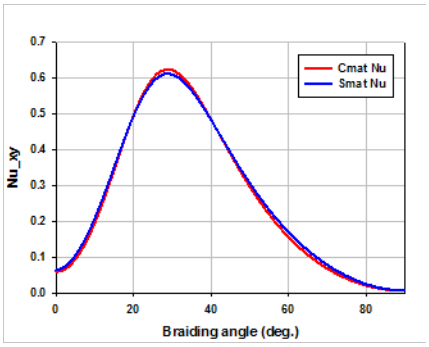
Cmat Nu
Smat Nu
Nu_xy
Braiding angle (deg.)

(d)

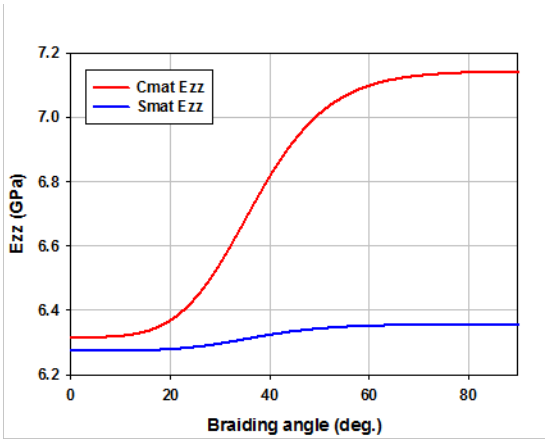
Cmat Ezz
Smat Ezz
Ezz (GPa)
Braiding angle (deg.)

(e)

Figure 2-9. Comparison between stiffness calculation and compliance calculation model. (a) fiber direction Young's modulus, (b) transverse direction Young's modulus, (c) shear modulus of XY direction, (d) Poisson's ratio of XY direction, and (e) thickness direction Young's modulus

Inner structure tracing is particular feature of FBM, so yarn orientation change is verified with simple tension model as Figure 2-10. It is represented by SDV3 value of ABAQUS output in this study. For tracing and validating of the orientation change, large deformation simulation is done. SDV3 value is radian and for example, Figure 2-10 is a 45 deg. 3D braided composite with 4 axis braiding. In this case, the angle change is shown form 45 deg. to 23.09 deg. At first of Figure 2-10, the braiding angle was started 44.51 deg. at 1.5 % elongation, next it was changed to 35.84 deg. at 15 % elongation, and finally it was 23.09 deg. at 30 % elongation according to tensile deformation. In this result, it was neglected that failure and Poisson's effect of the composite, however the mechanism is same with full analysis of the composite with FBM. According to this validation, off axis yarn angle is traced in other simulation results.

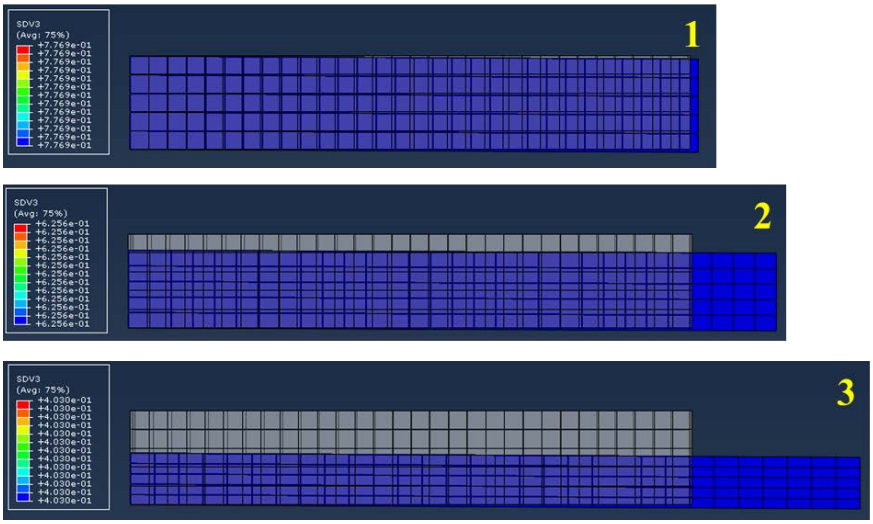

Figure 2-10. Braided angle change tracing according to state variable in ABAQUS during deformation in 45 deg. 3D braided composite. Form 44.51 deg. at 1.5 % elongation to 23.09 deg. at 30 % elongation.

Figure 2-11 is example of partial damage and total damage of the composite in the simulation. This is also particular feature of FBM and it is based on Puck's failure criterion. According to SDV1 and SDV2 partial failure and mode can be defined. As Figure 2-11, partial damage is occurred first as Figure 2-11(a). Here, failure mode can be defined with SDV1 value and SDV1 is defined tensile transverse failure of a layer. This figure is braided composite and transverse failure is detected in the off axis yarn first. Next the damage and failure mode is propagated and it is reflected on SDV1 as the value of 3 as Figure 2-11(b). It means tensile fiber failure and it occurs at axial yarn layer. Finally all layer is damaged and total failure is detected on SDV2 as a value of 1 as Figure 2-11(c). These two features is used for mechanical analysis of 3D textile composite and it is presented at section 4.

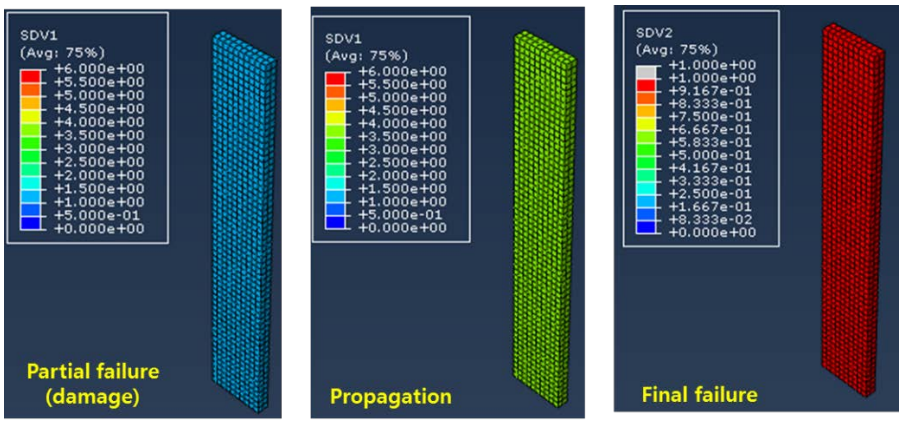

(a) (b) (c)

Figure 2-11. Partial damage and propagation example of 3D braided composite. (a) Partial damage initiation as transverse crack (SDV1 = 1), (b) damage propagation and tensile failure as partial damage (SDV1 = 3), and (c) total failure of a composite (SDV2 = 1)

2.3.2 Verification of mechanical properties prediction

Before using FBM for analysis 3D textile composite properties, it was compared to 3D unit cell analysis result for validation of its prediction accuracy. In this study, 3D orthogonal unit cell model is designed and simulated with simple tension condition. Figure 2-12 is 3D unit cell model and its simulation result. Here, carbon fiber properties is used with 30 % fiber volume fraction and the structure is ideal as Figure 2-12(b). Each direction yarn fraction is X:Y:Z=4:4:1 and each yarn is designed with straight orientation. Figure 2-13 is simple rectangular model for FBM analysis and its test result. this structure is simple rectangular shape and assumed perfect structure so failure occurs same

time on whole sample region. Stress-strain behavior of two models is Figure 2-14 and it shows FBM result shows similar accuracy with 3D unit cell model for mechanical properties of 3D textile composites. the Young's moduli of two model are 49.906 and 48.765 GPa.

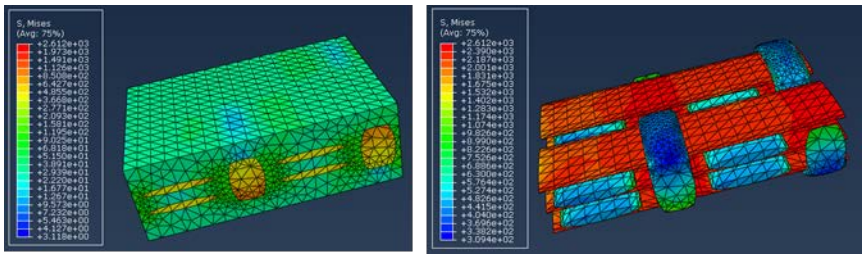

(a) (b)

Figure 2-12. Typical 3D orthogonal woven composite model and its simulation. (a) Stress distribution with simple tension and (b) stress distribution on fiber structure

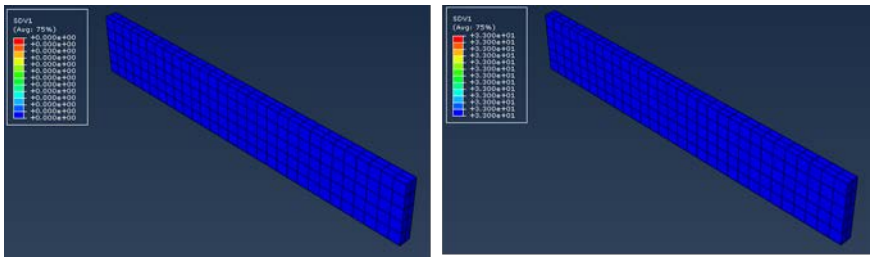

(a) (b)

Figure 2-13. Simple tension analysis model with FBM. (a) Rectangular sample shape and (b) test result with SDV value

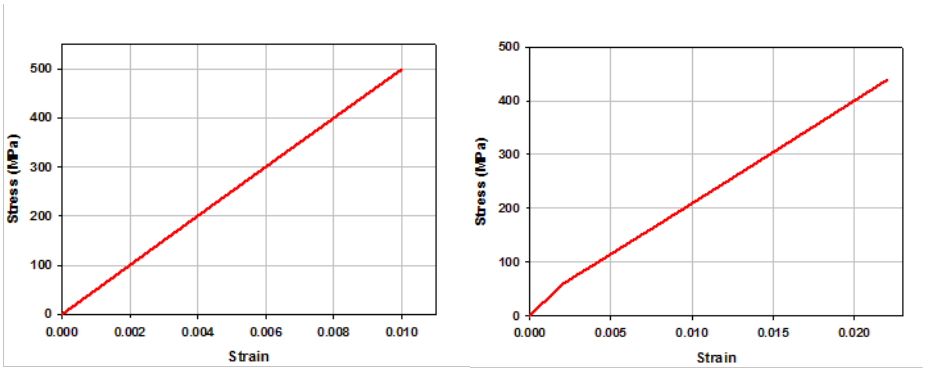

(a) (b)

Figure 2-14.Typical 3D orthogonal composite properties with numerical analysis. (a) 3D unit cell model and (b) FBM analysis result

2.3.3 3D structure calculation

Next verification is 3D solid analysis with complex shape for universal usage of FBM analysis model. Inner structure tracing by yarn orientation change Figure 2-15 is example analysis using FBM. It has concave and convex structure and consist of 3D five axis braided composite structures. Figure 2-15 shows compression behavior of 3D composite structures including inner structure change, partial damage and propagation. It shows FBM can be used for any 3D structure analysis with fiber-reinforced composite.

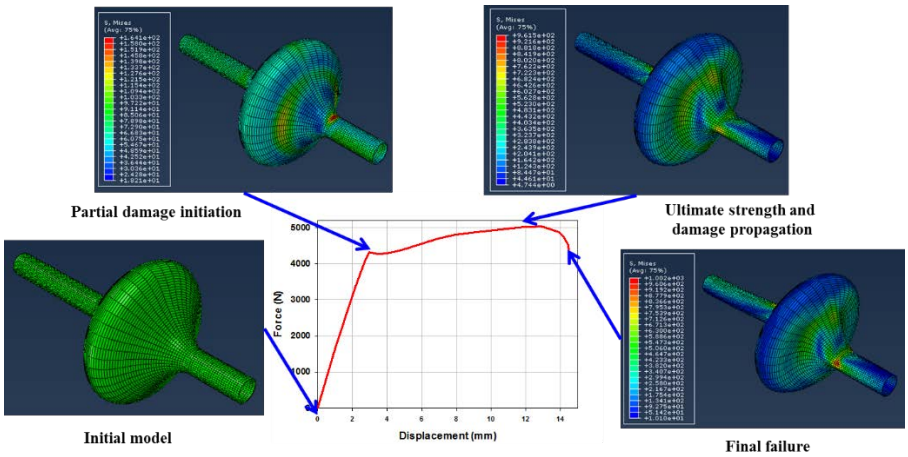

Figure 2-15. Example of 3D composite structure analysis with FBM

2.4Summary

In this chapter, new numerical approach method is developed called FBM. This method is continuum analysis considering fiber orientation and deformation for calculating mechanical behavior of 3D textile composite. Moreover, this method is not using unit cell structure analysis step, so one step analysis is available for 3D complicated textile structure with strength analysis. Fiber orientation and change is considered in stiffness calculation with tensor transform. Strength prediction is based on Puck's failure criterion and damage propagation model. Modified damage propagation model is used in this algorithm and it is applied with a type of ply discount model. Finally this method is implemented on commercial finite element software ABAQUS with user subroutine. In FBM analysis method, using fundamental material elastic modulus and strength, mechanical behavior of 3D textile composite can be predicted.

Chapter 3. Fabrication and modelling of 3D textile composites

3.1 3D braided structures

3.1.1 Fabrication of 3D five-axis braided preforms

3D textile composites is used for structural materials because they have no delamination, high failure strength, and long fatigue life with light weight. It is overcoming textile laminate weakness point however it is not easy to manufacture 3D preform with targeted structure and parameters. Braided composite is manufactured as five-axis structures with axial yarn. This composite has similar structure to tri-axial braided composites and it is extended to 3D structure of tri-axial structures. A manufacturing process of 3D five-axis braided composites is well-known process and its structure is also well established. In this study, based on these previous research four layer braided composites is manufactured. It is already used previous composites research and unit cell approach is considered at the previous research [2, 78]. The schematic diagram of braiding process is Figure 3-1.

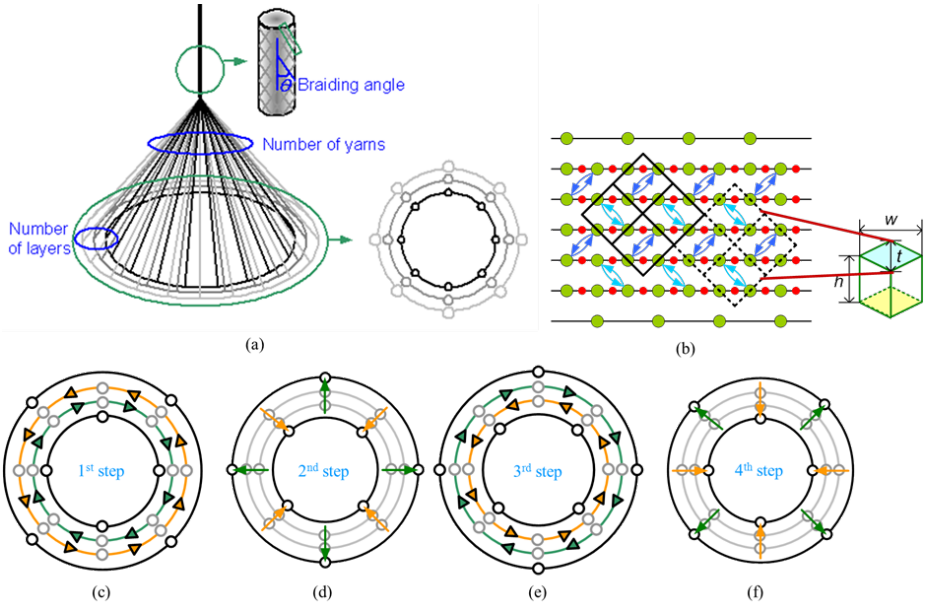

Figure 3-1. Schematic diagram of the braiding process (a) and motion of the yarn carriers: (b) overall, (c) first, (d) second, (e) third, (f) fourth steps in the formation of each unit cell. Red and green circles represent axial and braiding yarn carriers, respectively; solid box, unit cell after the first and second steps; dotted box, after the third and fourth steps [79]

The yarn carriers on concentric layers in the braiding bed move circumferentially; i.e., clockwise and counter-clockwise for each carrier in the odd and even layers, respectively (Figure 3-1(c)). The carriers then move radially; i.e., inward and outward for each carrier in the odd and even columns, respectively (Figure 3-1(d)). After these two steps, the carriers move in the opposite direction to the previous first and second steps, respectively (Figure 3-1(e) and 3-1(f)), completing a total of four steps. Considering these carrier motions, the repeating unit of the resulting braid can be identified schematically as shown in Figure 3-1(b).

As Figure 3-1, in this study, circular braided machine is used for making the sample, however, manipulating carrier motion, four layer rectangular sample is produced. For manufacturing braided preform, glass fiber (Dong-il Industrial Co., Korea) is used for this works. Table 7 is mechanical properties of fibers and resin used in this research. These material properties is based on industrial reference from each company and several values were used reference value and elastic assumption.

Table 7. Material properties of fiber and resin [29]

Martials	Modulus (GPa)	Poisson's ratio	Tensile strength (MPa)
Glass fiber	72	0.2	2,000
Carbon fiber	230	0.23	4,900
Epoxy resin	4.5	0.35	60

3.1.2 Unit cell and fiber based continuum modelling

The unit-cell of 3D braid scaffolds can be modeled mathematically, provided that the running paths of individual yarns inside the braid are determined by the manufacturing process (in this case, circular braiding) (Figure 3-1). 3D braid preforms were manufactured using the four-step process in a circular braiding machine built in a laboratory.

Two assumptions were made for the mathematical description of the unit cell: the braiding yarns in the unit cell are straight and their cross-sections are elliptical with major and minor radii of a and b, respectively. The geometrical description was then completed by mathematically expressing the actual

running paths of individual yarns. This description requires the unit cell size of the preform braid (width (w) x thickness (t) x height (h)), which can be determined using the braiding parameters and the physical dimensions of the target braid composite (Table 8). The axial yarn thickness does not affect the size of the unit cell. The width of the unit cell was determined from the number of braiding yarns per layer, while its thickness was calculated from the target composite thickness. The height of the unit-cell was calculated using the braiding angle, as follows Eq (3.1)

Table 8. Example braiding parameters and target composite dimensions

Braiding parameters	Layers of braiding	4
	Braiding yarn carriers per layer (n)	72
	Axial yarn carriers per layer	72
	Braiding angle (θ)	30°
Target braid dimension	Inner radius (R_i)	16.48 mm
	Outer radius (R_o)	17.91 mm
	Tube thickness (T)	1.43 mm

$$w = \frac{\pi(R_i + R_o)}{n} \times 4, \qquad t = \frac{T}{N+1} \times 4, \qquad h = \frac{w/2}{\tan\theta} \tag{3.1}$$

where N and n are the number of braiding layers and yarn carriers per layer, respectively. Θ, R_i, and R_o are representing the braiding angle and the inner and outer radius, respectively.

The meanings of characters in Eq. (3.1) are provided in Tables 8 and 9. Yarns were assumed to be elliptical. The radii of the ellipses were determined from the fiber volume fraction. The fiber volume fraction (v) in the unit cell can be calculated using the volume of the axial (Va) and braiding (Vb) yarns as Eq (3.2)

$$v(\%) = \frac{V_a + V_b}{V_t} * 100 \tag{3.2}$$

where $V_t (= wth/2)$ is the total volume of the unit cell. The volumes of the axial and braiding yarns are given by Eq (3.3)

$$V_a = 8(\pi abl), \; V_b = 8(\pi abh_0) \tag{3.3}$$

where l represents the length of the axial yarn in the unit cell and $h_0 = \sqrt{(w/2)^2 + (t/2)^2 + h^2}$. From the fiber volume fraction of the target composite, the product of the two radii (a, b) can be determined using Eq. (3.2). The radius of the short axis (b) is assumed to be $0.96 * t/8$ to prevent interpenetration between yarns (see Table 8 for detailed expression of each variable).

Based on these numerical model final model is Figure 3-2 and it is made by

TEXGEN that is textile structure design software. For FBM analysis, dimension of this model is used for the analysis and each orientation of the yarn in the composite is assumed that all of yarns have perfect orientation according to unit cell dimension. So the yarn structure is similar to tri-axial model except thickness effect.

Table 9. Unit cell geometry determined from the braiding parameters

Dimensions	
t (thickness)	1.1440 mm
w (width)	6.0022 mm
h (height)	5.1980 mm
a (major semi-axis yarn length)	0.5020 mm
b (minor semi-axis yarn length)	0.0661 mm
Axial yarn curve parameters determining axial yarn length ($l = \int_0^h \sqrt{1+(z')^2}\,\mathrm{dy}$, $z = A\sin\big(B(y-C)\big) + D$)	
A	0.1375
B	1.1589
C	0.6775
D	0.1375

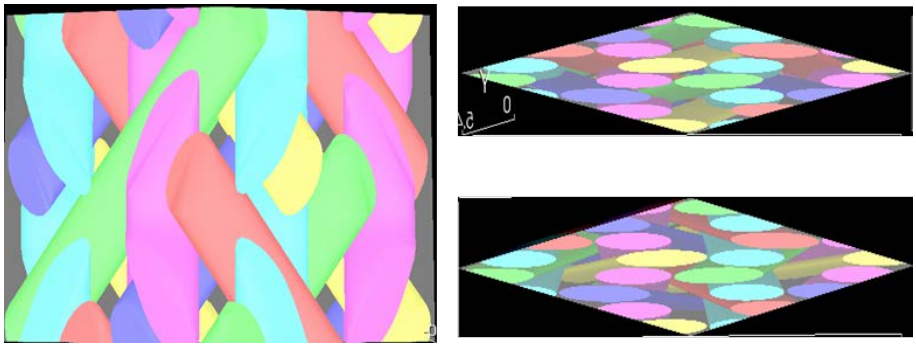

Figure 3-2. Geometrical model of a 3D braid preform unit cell with axial yarns [79]

3.2 3D orthogonal woven structures

3.2.1 Fabrication of 3D orthogonal woven preforms

In this chapter, 3D orthogonal woven composites is manufactured with new developed process jig. The new 3D woven jig consists of 3 major part as Figure 3-3.

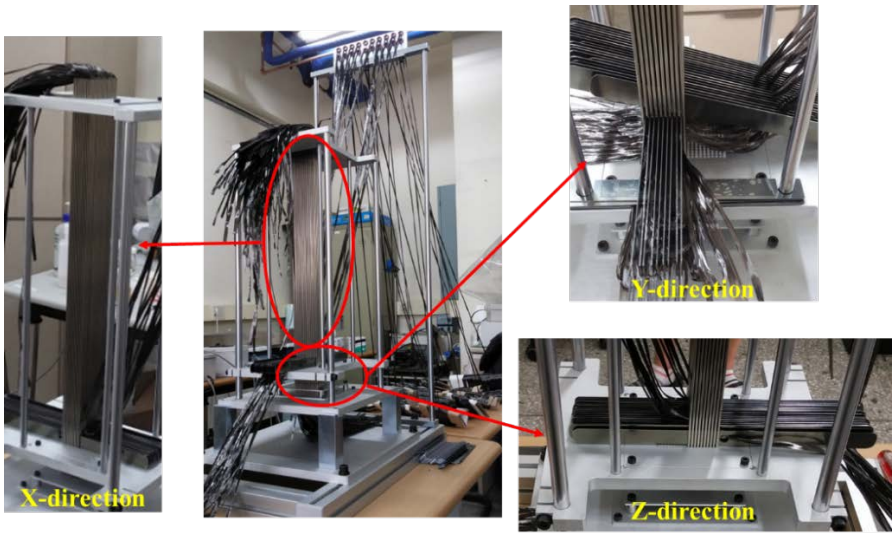

Figure 3-3. 3D orthogonal woven fabrication jig

First part is axial yarn tube as x-direction yarn component. A size and interval of this axial tube is one of parameters for fiber volume fraction of 3D woven composites. Next part is y-direction yarn part and it is consist of group of short fiber, the distance of fiber is defined by with of the composites. The last part is stitch yarn part and it consists z-direction yarn of the composites. This part is important part of the 3D woven composite because this stitch yarn is in tangled each layer of the yarns. The schematic motion of jig is Figure 3-4.

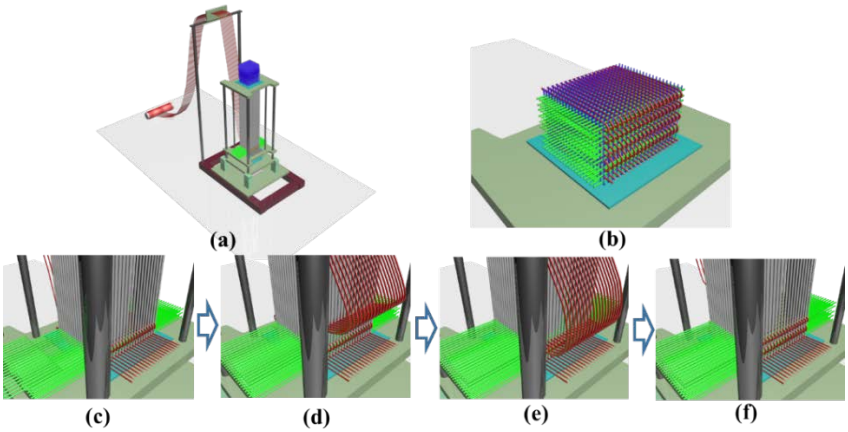

Figure 3-4. Fabrication motion of the jig. (a) overall structure of the jig, (b) sample structure of 3D orthogonal woven with the jig, (c) first inserting Y-direction, (d) first stitching of z-direction, (e) second inserting Y-direction, (e) second stitching of z-direction

Axial tube is set-up first including fibers (Figure 3-4(c)). After that weaving step is started. One weaving step consists of two y-direction yarn sets and two stitch of z-direction stitch yarn (see Figure 3-4(c)-(f)). The composite is manufactured by repeating of this step and it can be produced with continuum process with continuous fiber supplying of x-direction yarn. However, in this study, there is focused on manufacturing process and availability, so discontinuous sample is manufactured as mechanical test dimension. It is same to 3D braided composite manufacturing.

Based on this woven mechanism, 3D orthogonal woven preform was produced as Figure 3-5. Here 5 layer model is used with T700S grade carbon fiber (Torayca, Toray industries Inc.). Mechanical properties of fibers is also in Table 7 as above.

(a) (b)

Figure 3-5. 3D orthogonal woven preform and composite structures. (a) 3D preform with T700SC carbon fiber and (b) sample structure of the composite

3.2.2 Unit cell and fiber based continuum modelling

The unit cell of 3D orthogonal woven prepreg is also made by TEXGEN software. In this study, the yarn volume fraction is small, so the unit cell can be made with ideal yarn orientation and structure without interference.

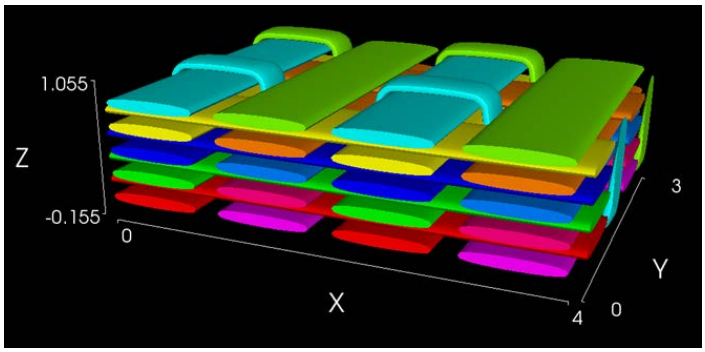

Figure 3-6. Ideal structure of 3D orthogonal woven composite

Figure 3-6 shows ideal unit cell structure of 3D orthogonal woven composite structure. The cross section of the yarn is calculated with carbon fiber filament

radius and number of filaments in the carbon fiber yarn.

For 3D woven model, using FBM analysis, there is needed defining stitch yarn path of the composite. Different from braiding yarn of braided composites, stitch yarn of woven composite path has more complex movement and effect to mechanical properties according to defining yarn orientation. Here, for mimicking this stitch yarn path, Furrier series square wave is used as Eq (3.10).

$$f(x) = \frac{4}{\pi} \sum_{n=1,3,5...}^{\infty} \frac{1}{n} \sin(\frac{n\pi x}{L}) \tag{3.10}$$

where the function is yarn path as square wave and L is length of the wave.

Here, the square wave is formed over 100 as value of n, however in FBM analysis differential is also important because that is angle parameter of the stitch yarn. Figure 3-7 shows the differences of angle change in the wave formula. Therefore, in this study, 1000 is used for n value and the step is one period of stitch yarn is separated as 200 steps. Figure 3-8 is final stitch yarn path and angle distribution of the yarn.

Based on this yarn orientation, 3D orthogonal woven composites FBM analysis model is defined with three layer system as Figure 3-9 and dimension of the composite is determined with manufacturing jig scale.

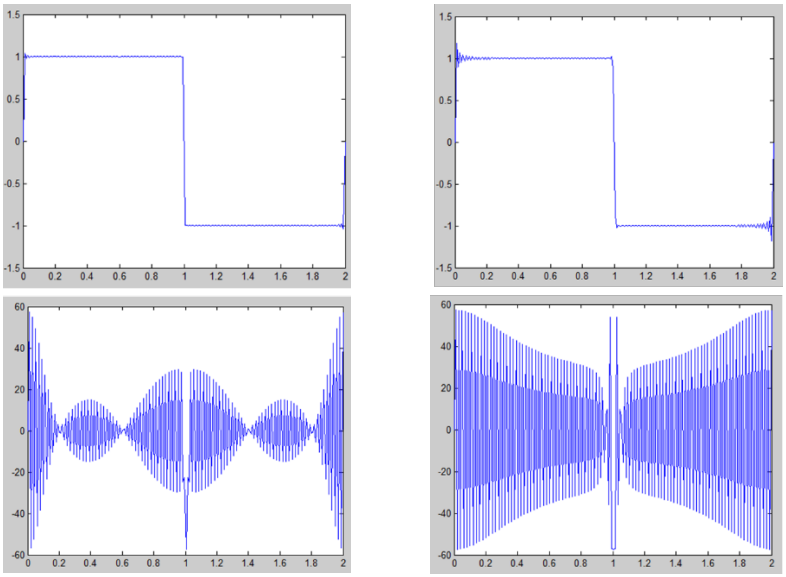

(a) (b)

Figure 3-7. Furrier series square wave function and angle change with L = 2.

(a) n = 500 case and (b) n = 100 case

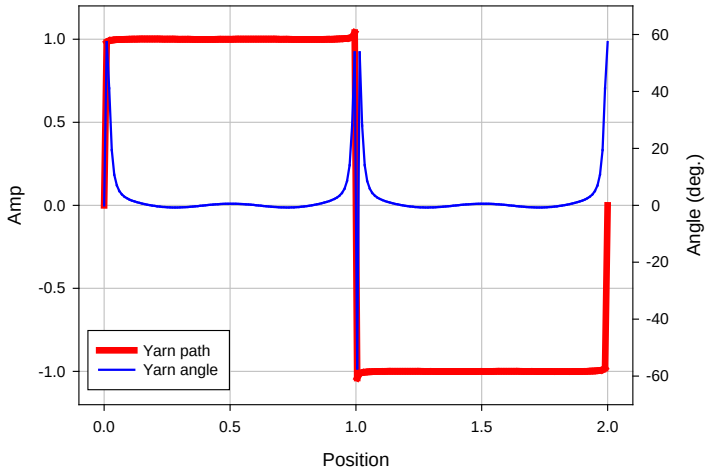

Figure 3-8. Selected Furrier series square wave function and its angle change

(n = 1000)

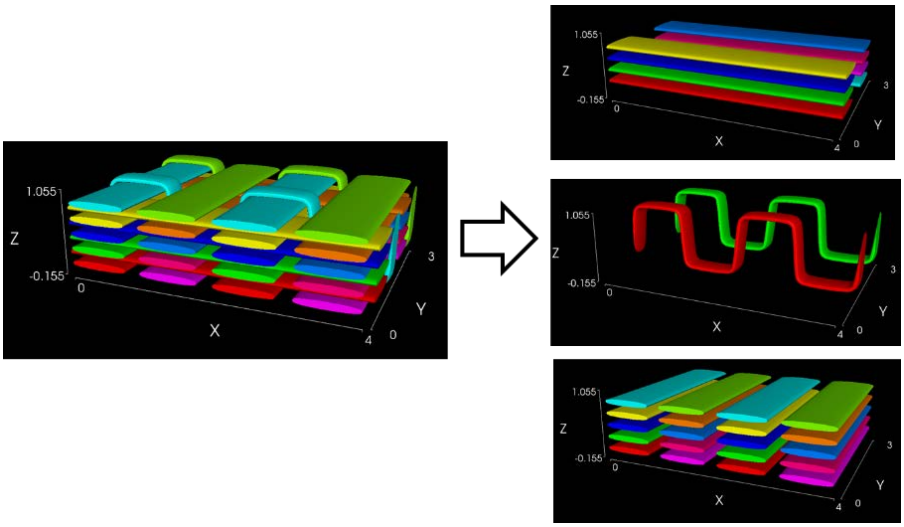

Figure 3-9. 3 Layers composition of 3D orthogonal woven composite for Layer method.

3.3 Forming and characterization of 3D textile composites

3.3.1 Vacuum assisted resin transfer molding (VARTM) process

Using 3D braided and orthogonal woven preform, composites are manufactured with vacuum assisted resin transfer molding (VARTM) process is used because the preform consist of yarn entanglement so simple press process cannot be avoided void and imperfection in the composite. Therefore, VARTM process is considered for reducing resin imperfection in composites with epoxy resin (Epofix, Struers). The resin properties is in above Table 7.

Not only 3D textile composite samples is manufactured, but also unidirectional composite is produced. For the unidirectional composites, tensile tests were carried out to obtain their elastic properties and failure strength. In

case of 3D composites, 3D braided and orthogonal woven composites are tested for characterization of the particular properties of 3D textile composites and validate of the numerical model. As I mentioned before, braided composite samples were fabricated, tested using glass fiber and orthogonal woven composite sample is used carbon fiber. Also, 3D braid preforms, which were prepared with a braiding structure of 4 layers and 12 carriers in each layer, were used. The braid angles were fixed to be 30 degree. In case of 3D orthogonal woven preforms, 5 layer model is used with uniform yarn density between x, y, and z direction yarns.

For unidirectional composites were fabricated using the press molding at 90℃ and 50 MPa because unidirectional composites are usually made with prepreg, however, using prepreg, there cannot be used same resin with other samples so we used press molding process for unidirectional composites. And the curing time of unidirectional composites was 30 minutes. Braided composites were then fabricated using VARTM process by immersing braid preforms in epoxy resin and removing the void in the resin by vacuum. For the validation works, 0, 45, 90 deg. glass fiber unidirectional composite samples and 3D braided glass fiber composite samples were tested. Fiber volume faction of all composite samples is manipulated about 45%. In case of 3D orthogonal woven composites, carbon fiber is used. It is same with braiding perform, unidirectional test is done for carrying out to obtain their elastic properties and failure strength. The 3D woven composite has large thickness and lower fiber volume fraction, so cannot be made with simple VARTM process as braided composites. Therefore new bottom up process and rein transfer mold was produced as Figure 3-10 using this mold, 5 layer 3D woven bulk is made with epoxy resin and the resin is same with braided composites.

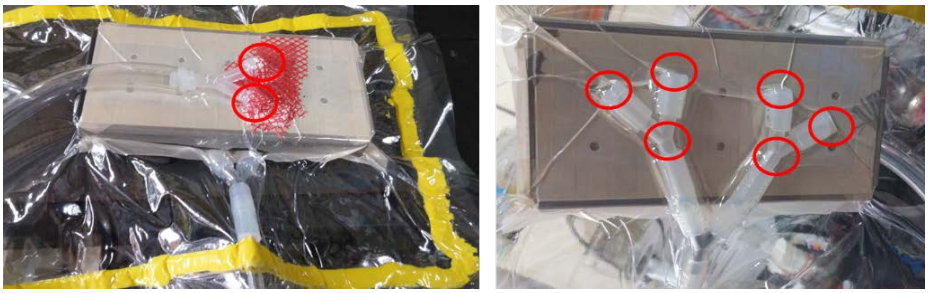

(a) (b)

Figure 3-10. Bottom up VARTM model and its structure. (a) top side, the red circle is air flow hole and (b) bottom side, the red circle is resin injection hole with 6 parallel ways.

Finally 3D textile composite samples were prepared as rectangular shape for mechanical test and characterization (see Figure 3-5(b))

3.3.2 Structure and material properties characterization

To verify the mathematical modeling of the unit cell, an optical microscope and computer tomography (CT) were used to observe the prepared specimens. For CT image, it is sensitive at density and material atomic structures, so Ultra-high molecular weight poly-ethylene (UHMWPE) fiber and epoxy composite sample is made and tested instead of glass fibers. UHMWPE fiber CT image condition is set in previous composite research, so we use UHMWPE fiber braided sample and carbon fiber woven sample is taken CT image. Therefore, in case of braided composite, the unit-cell geometry was constructed using TEXGEN as shown in Figure 5 and compared with experimental observations in Figure 3-11. Figure 3-11(a) shows the cross-sections of UHMWPE/epoxy

composites. The cross-sections of the braid and axial yarns in the braided composites appear not perfectly elliptical due to the compaction of filaments in the yarns; however, the positions of the two yarns in the braid composites were similar to the modeled ones. Figure 3-11(b) shows the internal structure of 3D UHMWPE preforms with and without axial yarns, comparing the modeled shapes with CT images, demonstrating that the unit cell modeling performed is highly suitable for mathematically describing the geometry of 3D braid preform and composites. In this braided sample case, real test sample is almost same with unit cell model, so fiber volume fraction and yarn path is use with simulated value.

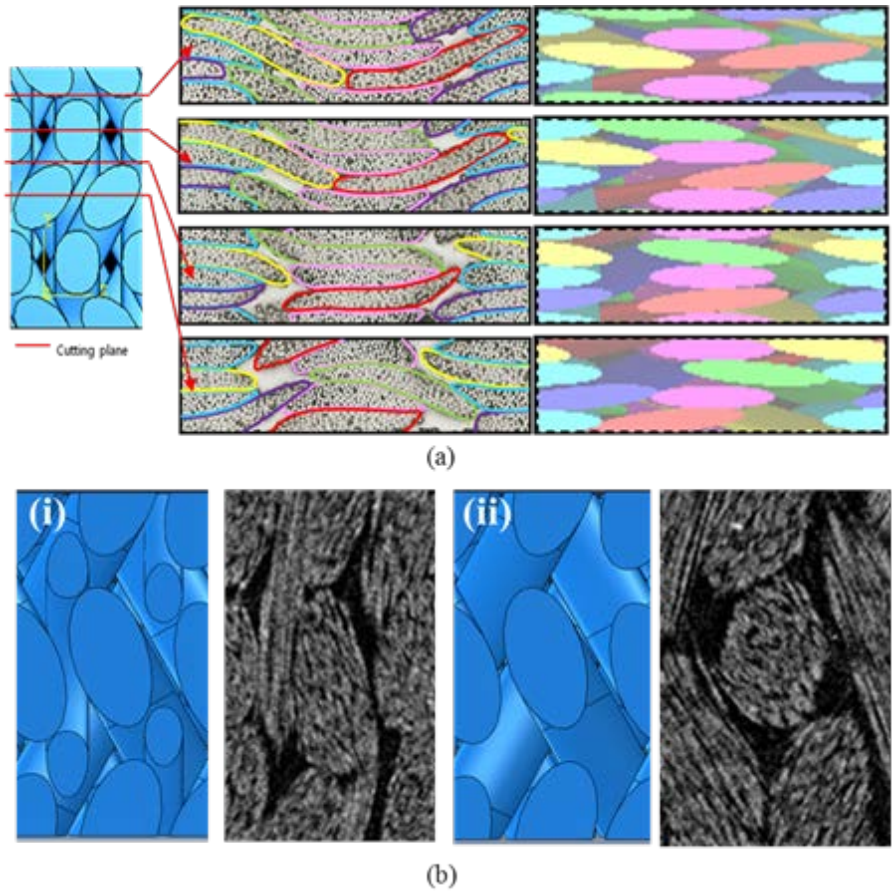

Figure 3-11. Cross sections of 3D braid composites. (a) SEM, and (b) micro-CT image (i) with and (ii) without axial yarns [79]

In case of 3D orthogonal woven composites, Figure 3-12 is inner structure of the composite samples by micro-CT. At Figure 3-5(b) shows optical view of composite sample and Figure 3-12 is internal structure with CT image. Different from braided composite, woven composite structure is not same with ideal case, however the composite sample has uniform structure and well made without critical imperfection. The fiber volume fraction of the composites is

calculated with yarn path assumption. X-direction and Y-direction yarn are assumed straight aligned and Z-direction stitch yarn is assumed having elliptical path. The ideal orthogonal structure and numerical model of is square shape. However real sample has very low fiber volume fraction and carbon fiber stiffness is very high, so stitch yarn is swelled so z-direction stitch yarn has elliptical shape path. Total fiber volume fraction is 17.9% and it is calculated by summation of each yarn density.

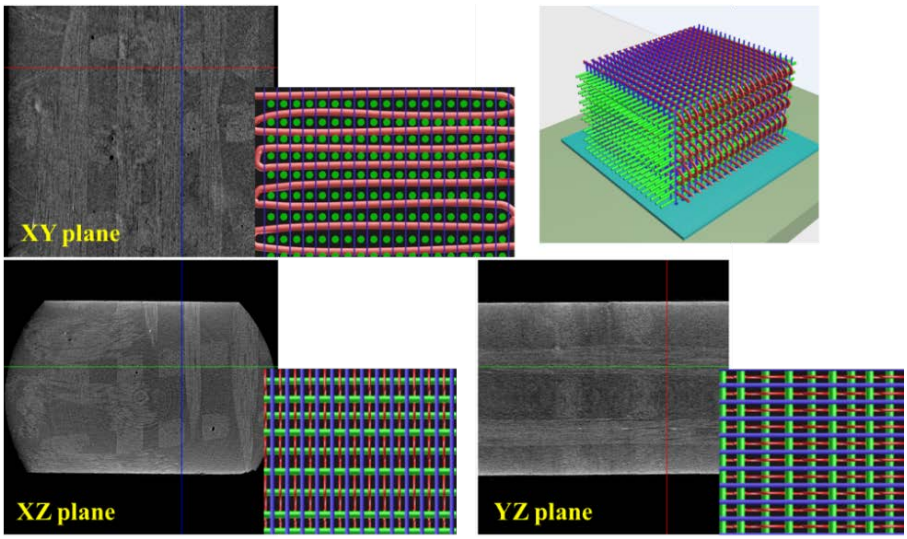

Figure 3-12. Micro-CT image of 3D orthogonal woven composite sample

3.4 Summary

In this chapter, 3D textile composites were manufactured with new fabrication method. At first, 3D braided composite is manufactured with axial yarn structure and its unit cell and FBM model is calculated. Here, 4 layer rectangular 3D braided preform is manufactured. In case of 3D orthogonal

woven composite, new fabrication jig is manufactured and it can be used for continuous 3D woven composite manufacturing. In this study, z-direction stitch orthogonal woven preform is manufactured. Using these 3D textile preform, composite were formed with VARTM process. Not only 3D textile composites, but also unidirectional composites is manufactured for fundamental material properties as modulus and strength. Moreover, using optical microscope and X-ray computer tomography, the inner structure of these composite samples was observed.

Chapter 4. Mechanical analysis of 3D textile composites

FBM analysis model is developed for textile composite analysis in this study. In this chapter, using FBM, 3D textile composite analysis was done. First, experimental study was done for characterization of 3D textile composites. Tensile and bending test was done with manufactured braided and orthogonal woven composites for mechanical behavior of the composites. Tensile and banding properties are fundamental properties of materials so basic properties of numerical analysis. For 3D textile composites, many research focused on unit cell approach because of its complex internal structure and various parameters [80]. Moreover, in these days, numerous numerical theories and technics is developed for textile analysis [41, 81, 82]. However, as chapter 2, FBM analysis method is different from other unit cell approaches, because this algorithm focused on continuum approach for whole composite structures. Therefore, using FBM, the analysis can be done that one step analysis with whole complex structures and textile design.

Based on experimental results, numerical validation work was performed. Fundamental material properties is defined with unidirectional test result and reference [75, 76]. 3D textile tensile and bending test result is compared to FBM numerical results. Moreover inner structure change (yarn orientation) and partial damage propagation is investigated in the 3D textile composites.

4.1 Experimental

4.1.1 Tensile test of 3D composites

The tensile behavior of textile composites were measured using universal test machines (Model 8801, Instron, USA) at strain rates of 0.002 s-1, respectively. For 3D braided composites were manufactured from glass fibers and epoxy resin matrix, also by unidirectional composites for fundamental material properties. For the tensile test, rectangular samples in 15 x 2 x 150 mm (width x thickness x height) were used. The specimens were pulled in the height direction with the clamping length of 30 mm. A preload of 20 N was applied to the specimens for stabilizing composite fiber structure. For 3D woven rectangular sample, the dimension is 6 x 12 x 150 mm (width x thickness x length) were used that is 2 times of unit cell with. The specimens were pulled in the length direction with the clamping length of 25 mm with testing tap. A preload of 20 N was also applied to the specimens for stabilizing. The test was done using universal test machines (Model 8801, Instron, USA) at strain rates of 0.002 s^{-1}, respectively. The representative experimental situation is Figure 4-1(a). The tensile test was done more 7 samples at each case and averaged without highest and lowest result. Unidirectional test result is just used modulus and strength value of 60% fiber volume fraction and other volume fraction and compressive value is used reference and assumption with simple rule of mixture. The value of used properties are longitudinal tensile and compressive strength, transverse tensile and compressive strength, and shear strength. 3D textile composite result is used as stress strain curve for characterizing the properties and compared to numerical analysis result.

4.1.2 Bending test of 3D composites

Three point bending test was carried out using same sample size with tensile test. Bending test was done with 3D textile composites only because unidirectional composite properties are just used for fundamental parameters with tensile and compressive strength value. Same samples with tensile test were used for bending test, so for 3D braided composites were manufactured from glass fibers and epoxy resin matrix and rectangular samples in 15 x 2 x 150 mm (width x thickness x height) were used. In the bending test, a preload of 5 N was applied to the specimens for stabilizing composite fiber structure. For 3D woven rectangular sample, the dimension is 6 x 12 x 150 mm (width x thickness x length) were used that is 2 times of unit cell with. Moreover, for the braided composite test, the support span is 120 mm and test speed is 2 mm/min and the head speed is calculated following ASTM D790. Also, flexible modulus and strength is calculated with same ASTM standards. In case of 3D woven textiles, 100 mm support span is used because of sample size and test equipment. The braided composite was tested test with universal test machine (UTM) as Lloyd instrument (LR50K, USA) and 3D orthogonal woven composite was tested with other UTM as Quasar 5 (Galbadini, Italy) due to laboratory condition. However, according to ASTM standard, the test condition is satisfied minimum condition of the test ratio. Test speed and calculation of properties was also done according to ASTM standard. Figure 4-1(b) shows representative test condition and the sample as before and after test pictures. Eq. (4.1) is flexural modulus and Eq. (4.2) is flexural strength from ASTM standard.

$$E_{flex} = \frac{L^3 F}{4wd^3} \tag{4.1}$$

$$\sigma_f = \frac{3PL}{2wd^2} \tag{4.2}$$

where L is gage length of a sample, F is slope of tangent to the initial straight line portion of load-deflection curve and P is load at a given point as ultimate strength. And w is width and d is depth or thickness of a sample.

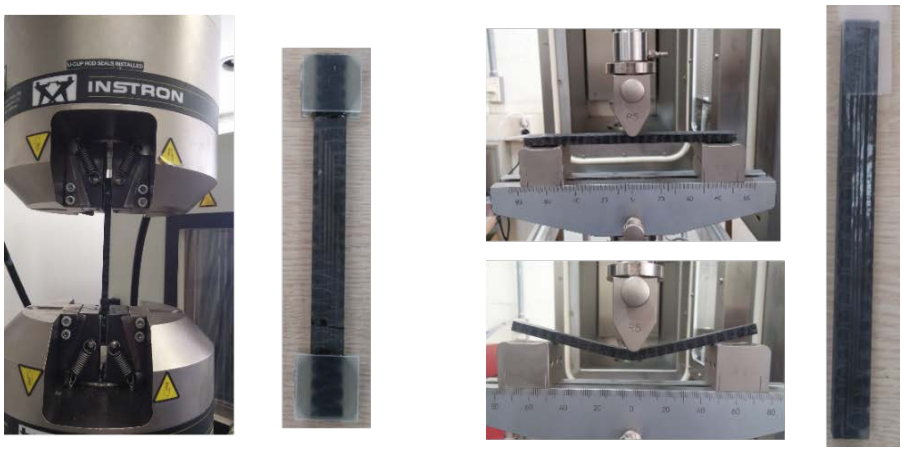

(a) (b)

Figure 4-1. Representative test condition of 3D textile composites. (a) Tensile test and (b) three point bending test

4.2 Theoretical analysis

For numerical analysis, the failure properties of the unidirectional composites were determined and provided as Table 10. All tensile properties are

experimental result and compressive data is assumed with reference [36, 83].

Table 10. Unidirectional composite properties [36, 83]

Materials (60 vol. %)	Longitudinal tensile (MPa)	Longitudinal compression (MPa)	Transverse tensile (MPa)	Transverse compression (MPa)	Shear (MPa)
Glass fiber	1,062	686	36	138	61
Carbon fiber	1,950	1,480	48	250	79

The unidirectional composite properties is defined at 60 % fiber volume fraction because of it is well used fiber volume fraction and tested in this study with press molding. However 3D textile composite has other fiber volume fraction such as 45 % for 3D five axis braided composite and 17.9 % for 3D orthogonal woven composites. In this case, the unidirectional composite properties at the volume fraction is calculated by interpolation with reference and assumed.

4.2.1 Simulation procedure and boundary condition

The simulation work is mimicked experimental study. Tensile and bending simulation is done with commercial finite element software ABAQUS using user subroutine. For tensile simulation, periodic boundary condition is applied because avoiding stress concentration error. The FBM method determined partial damage and propagation with stress tensor on the every element and applying stiffness degradation to partial damage element so edge boundary stress concentration can be effect to boundary element property degradation.

Periodic boundary condition is activated with input file treatment in ABAQUS software. Tensile simulation is done with same dimension with 3D textile composite samples with x-direction elongation. Stress-strain curve is treated by reaction force and displacement value. For mechanical behavior 5 % elongation result is gained with 0.05 % increment step. Checking angle variation and change, 30% elongation simulation was also done with 0.3% increment step and in this case, failure and damage is ignored because its deformation is already failure before 30 % elongation. In this research 3 state variable is used that additional information value of finite element analysis numerical simulation. They are called SDV and SDV1 as partial failure value, SDV2 as total failure value, and SDV3 is yarn angle from x-direction. In braided composite case, braided angle is recorded at SDV3 and in 3D orthogonal woven case, z-direction stitch yarn path angle is traced by SDV3 value. For SDV1, the SDV1 value is an integral number and each digit indicates each partial layer. SDV2 is final failure of a composite and it has a value over 1 means total failure of a composite. The failure angle can be also calculated based on Puck's criterion however it was processed in the subroutine and not treated output parameters. The failure mode can be defined by SDV1 variables. For bending simulation, periodic boundary condition cannot be used. So rigid body jig is manufactured. The contact properties of test part and jig part is treated as hard contact and friction. Here, 0.99 friction coefficient is used because of avoiding numerical error with assumption of simple contact condition.

4.2.2 Result treatment and post calculation

From numerical analysis, force and displacement data and SDVs value is gained. Stress and strain behavior of the composite is calculated using the force displacement relationship. Figure 4-2 is representative example of numerical result as 3D braided composite tensile simulation. As Figure 4-2 stress-strain behavior is gained and non-linear property was shown. An inflection point is

partial damage point and it is classified by SDV values. For example, in Figure 4-2, first inflection point is partial damage start point and it is determined transvers failure of braided yarn according to SDV1. After that non-linear increase occurs by inner yarn orientation change. The yarn orientation is traced as SDV3. Second inflection point is tensile failure of axial yarn and the axial yarn is dominant tensile properties, so tensile properties are depredate significantly. Finally braided yarn tensile failure with total composite failure. In this case, for axial yarn, no off-axis is occurred so axial yarn transvers failure is ignored until total failure. Also according to tensile loading, braiding yarn orientation change is traced as Figure 4-2. However, tensile deformation until failure of the braided composite is small as unidirectional composites, so not significant angle change is occurred.

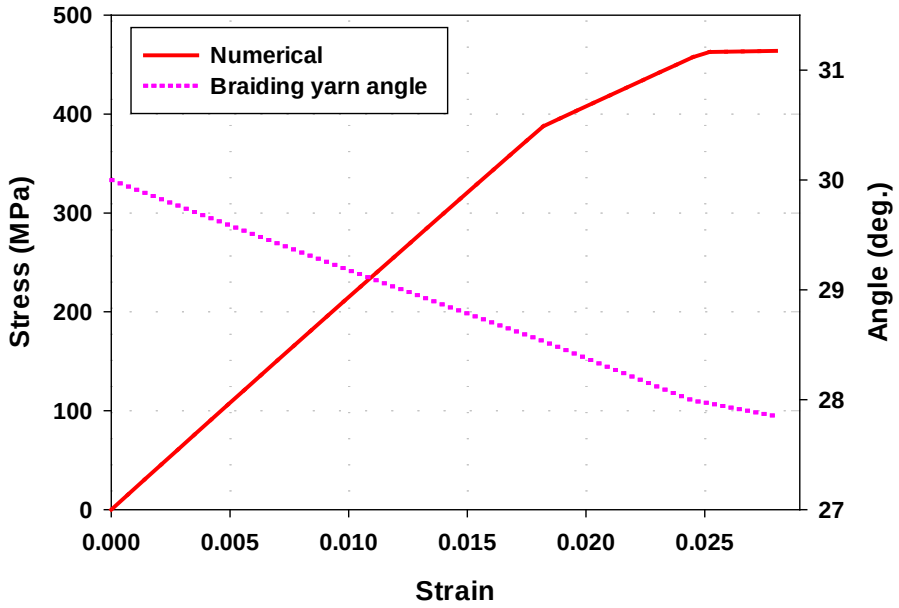

Figure 4-2. Representative numerical result of 3D braided composite

For bending simulation, flexural stress and strain behavior is calculated using

reaction force of upper jig and sample displacement. It was also calculated with force displacement relationship of numerical result. Here, slip in contact region is neglected in this study.

4.3 Results and discussions

4.3.1 Experimental results

Figure 4-3 shows braided composite tensile test results and bending test results. Each test is done with more 7 samples and averaged excluding highest and lowest value. The composite modulus, failure strength and failure strain is Table 11. Moreover Figure 4-3 is pictures of before and after test samples. In the tensile test of braided composite case, non-linear degradation behavior is shown and it is due to stimulus damage and propagation in a composites such as micro-crack and yarn failure filament by filament. Its failure strain is similar to unidirectional composite, because tensile properties of 3D five axis braided composite is mainly controlled by axial yarn property and it is longitudinal aligned as yarn of unidirectional composites. At the failure, braiding composite is totally failed as all of yarn part is broken. For bending test of braided composite case, its non-linear behavior is smaller than tensile case. It seems to inner deformation of the composite is smaller than tensile case. The flexural strain is also smaller than tensile deformation. Moreover, bending failure of the composite not total failure of the yarn and it is type of de-bonding failure (See Figure 4-4(b). Due to this reason, flexural strain is also much lower than tensile strength. Yarn undulation of a braided composite is not large effect for bending properties so its bending behavior is similar to unidirectional composites. However, a braided composite has yarn entanglement so matrix transverse crack and de-bonding occurred before yarn failure. And its toughness is higher than unidirectional composite due to this effect. This effect also detected on the numerical simulations.

Table 11. Experimental result of 3D textile composites

Structures	Five axis braided composite	Orthogonal woven composite
Materials	Glass fiber	Carbon fiber
Fiber volume fraction	45 %	17.9 %
Tensile properties		
Young's Modulus (GPa)	21.73 (1.31)	16.781 (0.077)
Failure strength (MPa)	471.21 (29.52)	231.26 (8.85)
Failure strain (%)	0.029 (0.002)	1.98 (0.11)
Bending properties		
Flexural Modulus (GPa)	19.122 (1.04)	17.815 (1.005)
Flexural strength (MPa)	144.31 (10.35)	269.12 (14.38)
Failure strain (%)	0.00943 (0.0005)	2.21 (0.13)

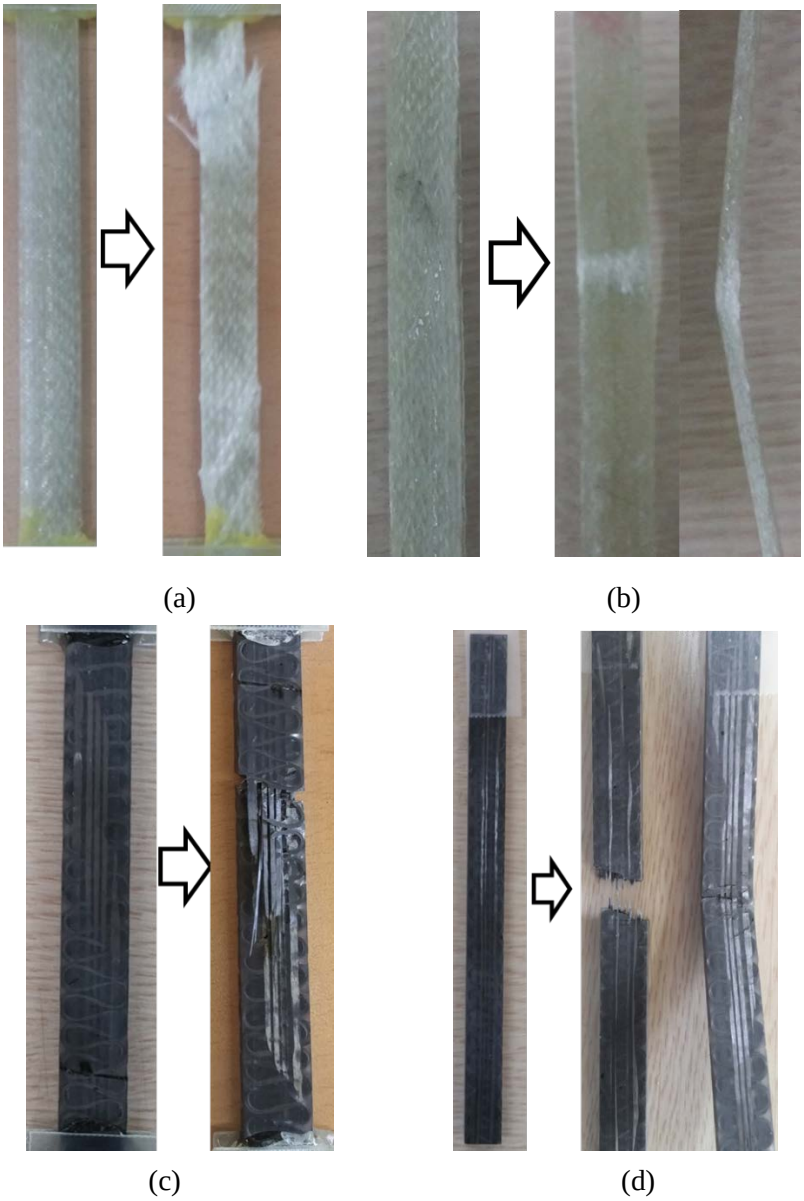

Figure 4-3. Test before and after samples of 3D textile composites. (a) Tensile test of braided composite, (b) bending test of braided composite, (c) tensile test of orthogonal woven composite, and (d) bending test of orthogonal woven composite

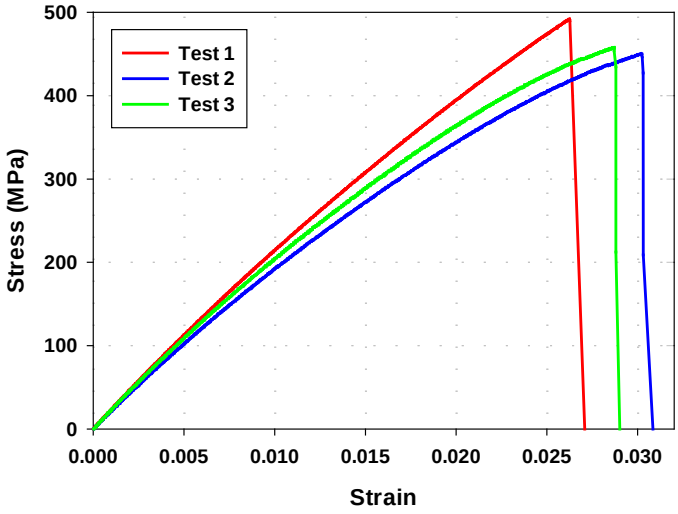

(a)

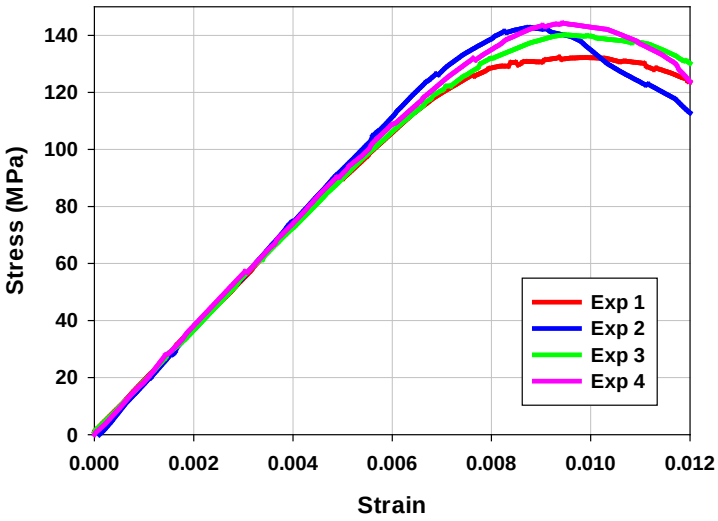

(b)

Figure 4-4. Representative test result of 3D textile composite samples. (a) Tensile test and (b) three point bending test

In 3D orthogonal woven composite case, the test result is Figure 4-5 and test sample pictures is in Figure 4-3(c) and (d). Figure 4-5(a) is tensile test result of woven textile composite. Similar to braided composite test, non-linear behavior is shown and partial failure effect is occurred. Moreover, according to elongation, 3D woven composite has more stimulus crack is investigated because of 3D woven composite has more transverse interface according to loading direction than braided composites. Also almost yarn is aligned to rectangular coordinates, critical partial damage that is significantly effect to stress-strain behavior is not detected. For three point bending test, the test result has complicated stress-strain curve due to Z-direction stitch yarn. As Figure 4-5(b) similar to other aligned composites, a 3D woven composite has linear fitted stress-strain behavior until first critical partial failure, however after that, complex deformation and damage propagation behavior is shown. 3D woven composite has Y and Z direction yarn as transverse direction, so based on transverse crack, non-linear behavior and multi-step failure is existed. And more, Z direction stitch yarn has elliptical path and it shows particular behavior as Figure 4-5(b). Moreover, due to this particular properties of 3D woven composites, the composite has high toughness after ultimate strength. Here, stress-strain behavior is shown until ultimate strength as about 2 percent deformation, however final failure is appeared over 3 percent. Furthermore, differently unidirectional or braided composite, 3D woven composite has Z direction stitch yarn, so thickness direction de-bonding and delamination effect is lower than other structures. The modulus and strength is in Table 11 and the result shows higher bending properties than other textile composites even this sample has low fiber volume fraction. The property is almost uniform structure behavior as steel or ceramic between tensile and bending behavior and these properties shows 3D woven composite structure can be useful for structural materials for sustaining complex load condition. Moreover, 3D woven composites have high toughness and it is also merit for structural materials.

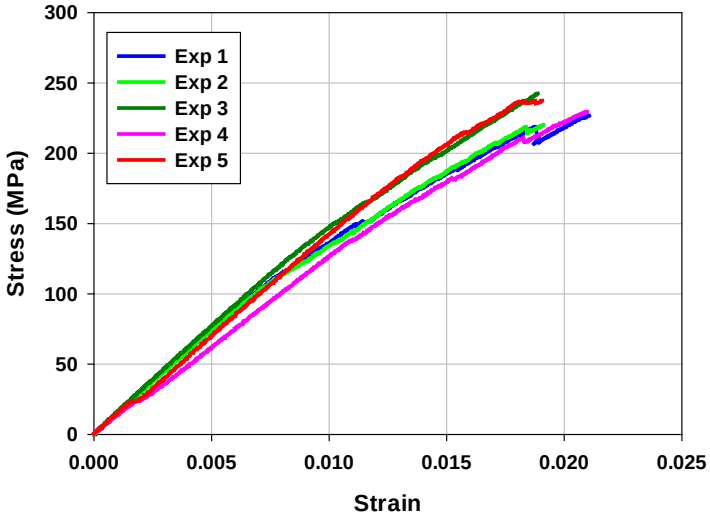

(a)

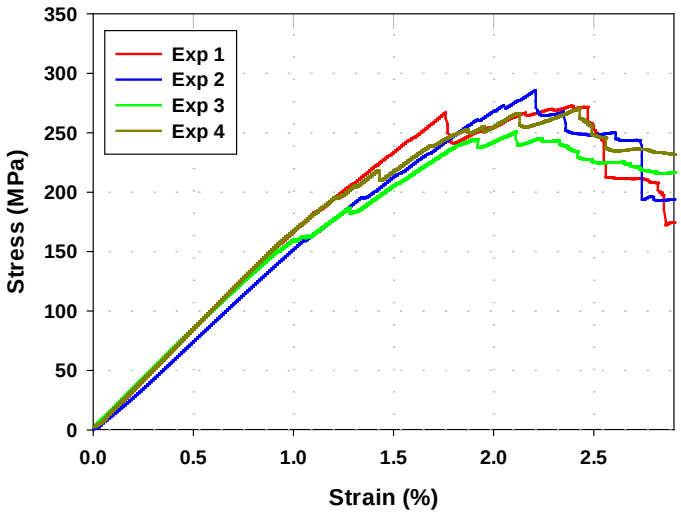

(b)

Figure 4-5. Representative test result of 3D orthogonal woven textile composite samples. (a) Tensile test and (b) three point bending test

4.3.2 Numerical results and comparison

Numerical analysis was done with FBM analysis model. According to section 4.3, unidirectional composite properties used for failure condition prediction. Based on these fundamental parameters, numerical analysis of 3D textile composite was done. 3D five axis braided and orthogonal woven textile composite simulation were done. Figure 4-6 is braided composite tensile test and its comparison result. As Figure 4-6 numerical prediction is well matched experimental result and its stress-strain behavior is well mimicked with elastic and inner structure update. Moreover, as section 4.3, inside of a composite change is predicted as braiding angle change and partial damage propagation. According to deformation, longitudinal elongation is occurred and braiding yarn was longitudinally aligned as braiding angle reducing. In this case, 30 deg. braiding angle was reduced 27.8 deg. until failure. Accruing to braiding angle change, transverse crack occurred first. Before partial damage as transverse crack, stress-strain curve is slightly increased that linear behavior because of reduced braiding yarn angle. After partial failure occur, stiffness degradation is detected by modified ply discount model. After that, more deformation was proceeded and critical damage is occurred as axial yarn tensile failure. Tensile load is sustained by axial yarn, so after axial yarn broken, composite stiffness significantly degraded and total composite is failed shortly. The FBM analysis model is designed that the code is stopped after total failure, so the stress-strain curve is finished at total failure point. The comparison between numerical and experimental result is Table 12.

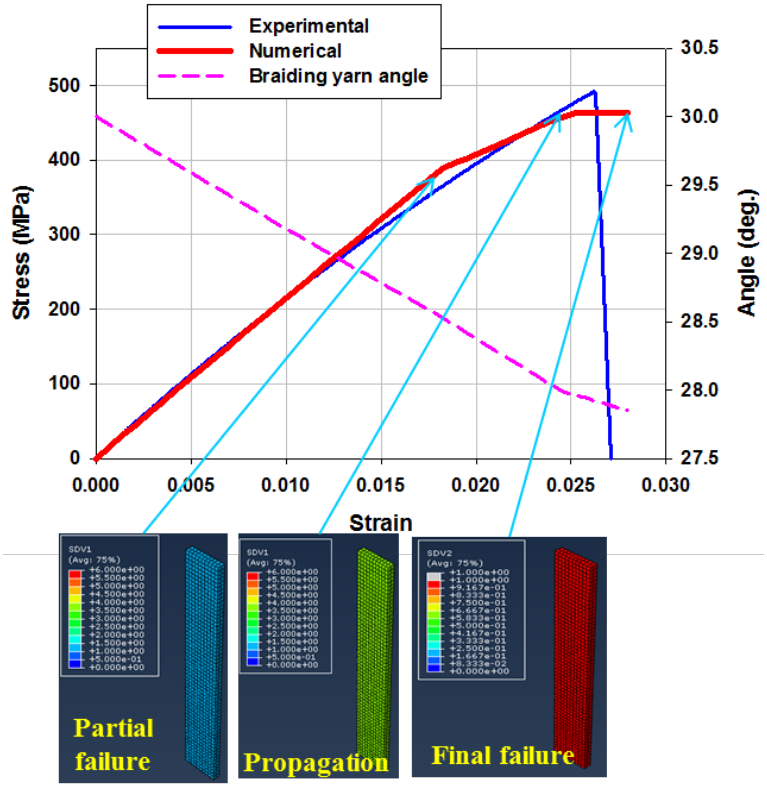

Figure 4-6. Tensile behavior of 3D five axis braided composite and its comparison between numerical and representative experimental result.

Table 12. Comparison between numerical and experimental results of 3D textile composite

Structures	Five axis braided composite		Orthogonal woven composite	
Tensile properties	Exp.	Numerical	Exp.	Numerical
Young's Modulus (GPa)	21.73 (1.31)	21.70	16.781 (0.077)	16.829

Failure strength (MPa)	471.21 (29.52)	463.88	231.26 (8.85)	251.68
Failure strain	0.029 (0.002)	0.028	0.0198 (0.0011)	0.022
Bending properties				
Flexural Modulus (GPa)	19.122 (1.04)	19.386	17.815 (1.005)	19.219
Flexural strength (MPa)	144.31 (10.35)	161.56	269.12 (14.38)	291.26
Failure strain	0.00943 (0.0005)	0.00903	0.0221 (0.0013)	0.0210

Bending simulation result and comparison is Figure 4-7. Bending simulation was not used periodic boundary condition so non-uniform stress distribution is shown. Also partial failure was propagated as Figure 4-7. Bending behavior of braided composite was particular process as non-total failure. As Figure 4-3(b), the matrix was failed totally, however fiber is not broken until displacement limit. After test, the sample was not broken until 90 deg. curvature. It means fiber-matrix is totally de-bonded and cannot flexural load transfer. So in experimental result, the composite has ultimate strength about 0.9 % bending, however still flexural load is sustained until bending limit. It was also in numerical result, the partial failure occurred before ultimate strength as transverse matrix failure and all layer transverse failure occurred at ultimate strength. After ultimate strength point, the stress in decreased however total failure is not occurred until simulation finished that is 10 % flexural deformation. For linear region, instead slightly increasing phenomenon is not shown, stimulus decreasing is detected because damage propagation is proceed as real situation due to rigid jig part is used as experimental. That means the numerical solution is well mimicked experimental condition. In figure 4-7,

numerical result until 1 % deformation is included because after 1 %, the numerical result has not meaningful data due to stability of FBM analysis code. However the result is well matched with experimental data. The comparison value between numerical and experimental result is Table 12. Its error is bigger than tensile test especially strength estimation, however it is about 10 % difference and acceptable value. Furthermore, the more reason of result is imperfection of the test sample because bending test is more sensitive about void or internal crack than tensile test by tension and compression coupling effect. Moreover, in this study, we assumed that composites has no de-bonding at the interface, however in the bending test, crazy and delamination at the interface is important factor for determining strength of composites.

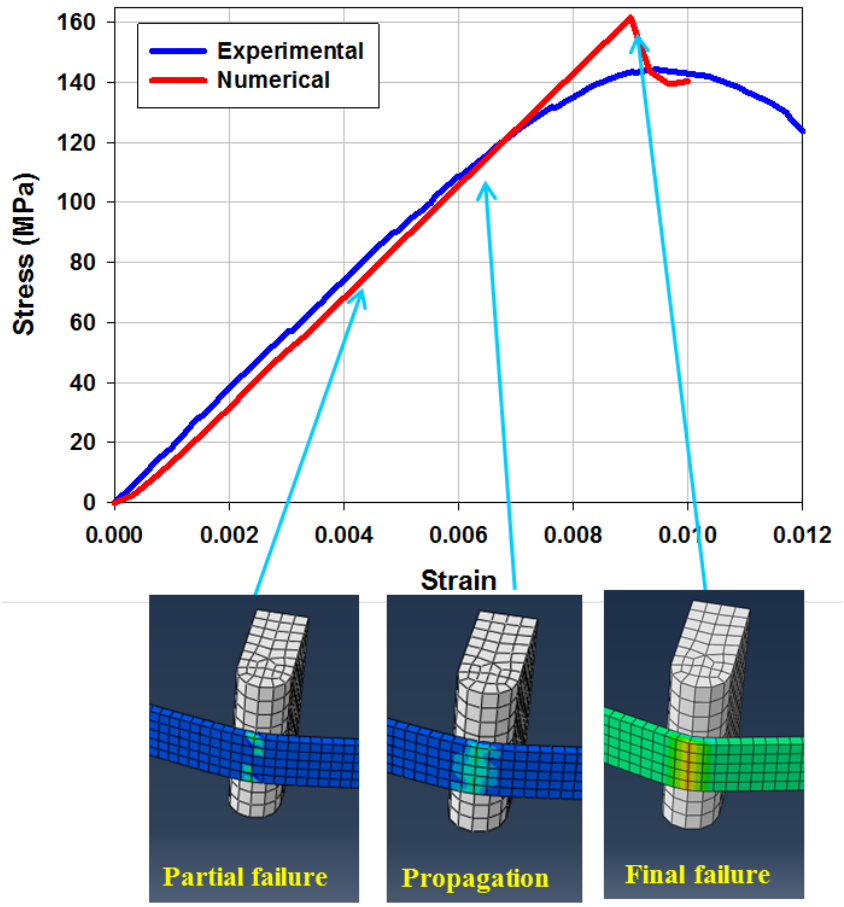

Figure 4-7. Flexural behavior of 3D five axis braided composite and its comparison between numerical and representative experimental result.

In 3D orthogonal woven composites, the numerical result and comparison is Figure 4-8. For 3D woven composite results, the numerical simulation specimen is similar to braided composite, so SDV as damage propagation figure is omitted and explained with graph result. 3D woven composite consist of 3 layer part and Z direction stich yarn is not easy to failure simulated because Z direction yarn is angle treatment and averaged stiffness properties was inputted.

So first partial failure is Y direction yarn transvers failure. Also according to deformation, stitch yarn angle variation is reduced due to alignment by elongation. So here is also slightly increasing behavior is shown similar to braided composite tensile simulation. for final failure, x direction yarn fiber failure is final failure of a composite and Z direction stich yarn is also failure at this point because load sustaining carriage of X direction yarn is larger than Z direction stitch yarn, so after X direction yarn failure stich yarn cannot sustaining the load alone and failure immediately after X direction yarn tensile failure. So the numerical result shows bi-linear like behavior with slightly non-linear increasing properties. Young's modulus and failure strength of 3D woven composite were well predicted with FBM analysis and the value of result is Table 12. However, in experimental non-linear decreasing is shown according to elongation due to stimulus de-bonding effect between fiber and matrix and it was investigated by sound during the experimental. Bending simulation was also done and compared. Figure 4-9 and 4-10 shows bending result and comparison between numerical and experimental result. Minus value of SDV1 at figure 4-10 is treatment error and it was changed zero immediately before next increment. At section 4.4.1, particular bending behavior of 3D woven composite was explained and it was repeated in simulation result. Different form braided composite, woven composite shows stimulus decreasing behavior according to deformation. For bending deformation, yarn angle change is smaller than tensile deformation and moreover, 3D woven composite has Z direction stitch yarn effect for non-linear properties. For the ultimate strength point, 3D woven composite has total failure, however a ultimate strength occurred with X direction yarn failure. Total composite failure is shown after ultimate strength with Z direction yarn failure. The value of modulus and strength is Table 12 and its prediction is well matched without 3D unit cell approach. From 3D braided and orthogonal woven composite simulation, FBM analysis method is well predicted mechanical behavior of 3D textile composite just using fiber and matrix properties with internal fiber structure update.

However, non-linear properties of stimulus failure cannot be traced using current model. It is needed modified layer model or stochastic model for this properties. Nevertheless of this limitation, stress-strain curve is predicted within about 10 % error form initial to total composite failure strain.

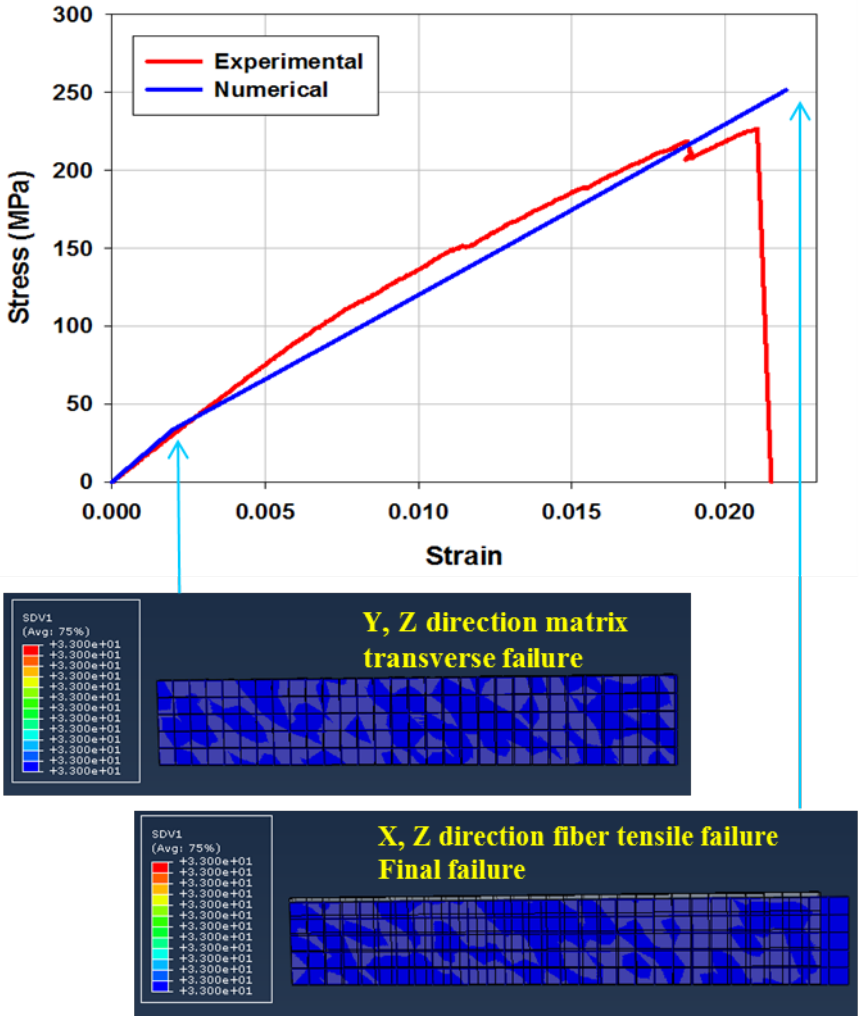

Figure 4-8. Tensile behavior of 3D orthogonal woven composite and its comparison between numerical and representative experimental result.

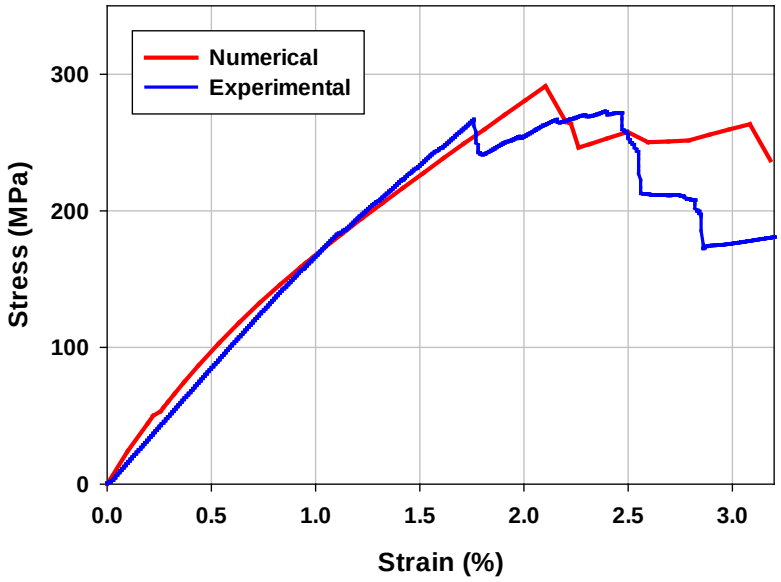

Figure 4-9. Flexural behavior of 3D orthogonal woven composite and its comparison between numerical and representative experimental result.

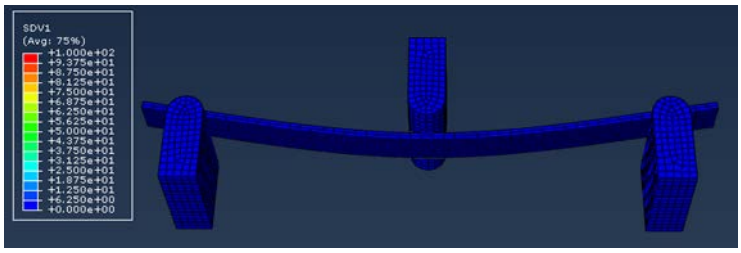

(a)

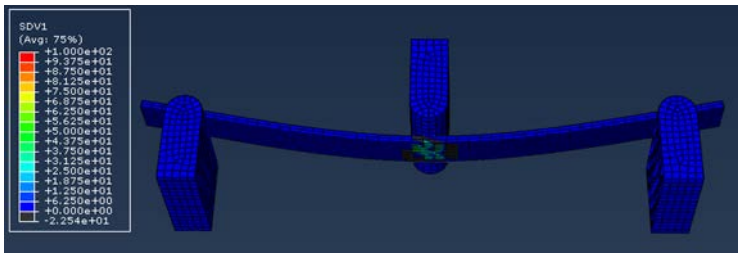

(b)

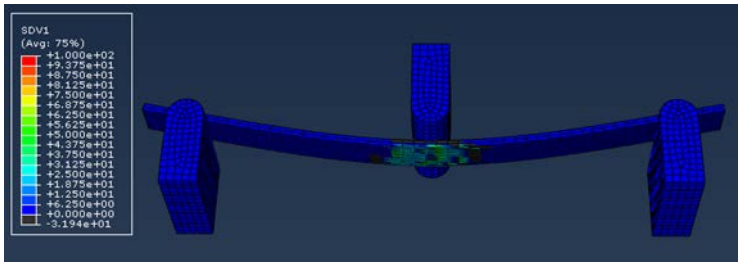

(c)

Figure 4-10. Damage propagation of 3D orthogonal woven composite at three point bending test

Using FBM analysis, comparison of 2D woven composite, 3D braided composite and 3D orthogonal woven composite. Figure 4-10 shows tensile behavior of three types of composite with same fiber volume fraction. 3D orthogonal woven composite has 17.9 percent of fiber volume fraction and it is lowest fraction of composites in this research, so fiber volume fraction is set 17.9 percent and carbon fiber properties was used this simulation. As Figure 4-11, 2D woven composite has highest modulus and strength due to longitudinal direction fiber portion is more than other structures. 3D woven composite is shown middle range modulus and strength due to Z direction stitch yarn is aligned rectangular coordinated direction so stitch yarn carried higher load than off axis yarns in braided composite. due to these off axis braided yarn, 3D braided composite has lowest modulus, however these braiding yarn sustain

more load after tensile yarn failure so failure strain of braiding composite is larger than other structures.

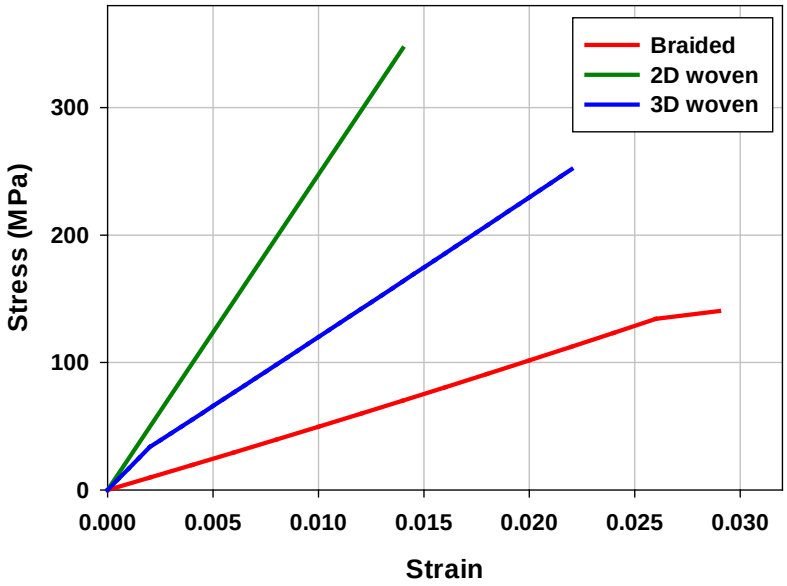

Figure 4-11. Numerical comparison of 3 types textile composite with same dimension and fiber volume fraction as CFRP

4.3.3 Discussions and applications

FBM analysis was done and compared with experimental study. This method well predicted mechanical behavior of 3D textile composite based on fiber and matrix properties considering inner fiber orientation update. However, it is mentioned section 4.4.2, non-linear properties of stimulus failure cannot be traced using current model. For solving this problems, modified layer model or stochastic model is required and it is not considered in this study. Nevertheless

of this limitation, stress-strain curve is predicted within about 10 % error form initial to total composite failure strain. Moreover FBM analysis method can be used directly 3D structure analysis and predicted mechanical behavior of 3D composite structures. Figure 4-12 is an example of numerical analysis of 3D woven composite used. Previous research, its properties are estimated with unit cell modelling result and combination with another step of structural analysis. However, in this study, FBM analysis method is used and directly analyze its mechanical properties with fiber and matrix properties. Figure 4-12 is 2D and 3D woven composite comparison example with carbon fiber reinforced composite structure. Fiber and matrix were assumed same with 3D orthogonal woven analysis sample and fiber volume fraction is also same with 3D woven test sample. As Figure 4-12(a) 3D woven composite model has less stress concentration and failure strain is higher according to 4-12(b). The reason of result is stitch yarn effect to torsional reinforcement. 3D woven composite has Z direction stitch yarn and higher torsional performance. This example structure is screw blade and high torsional properties are needed, so 3D woven structure is good for a type of blade structures. In this example, 2D woven model was 132 MPa failure strength, however 3D woven composite was endured 152 MPa stress at same deformation with same boundary condition.

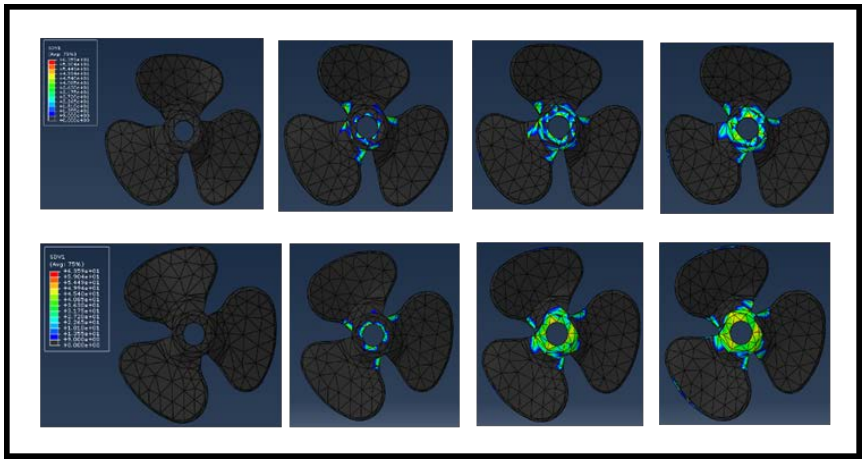

(a)

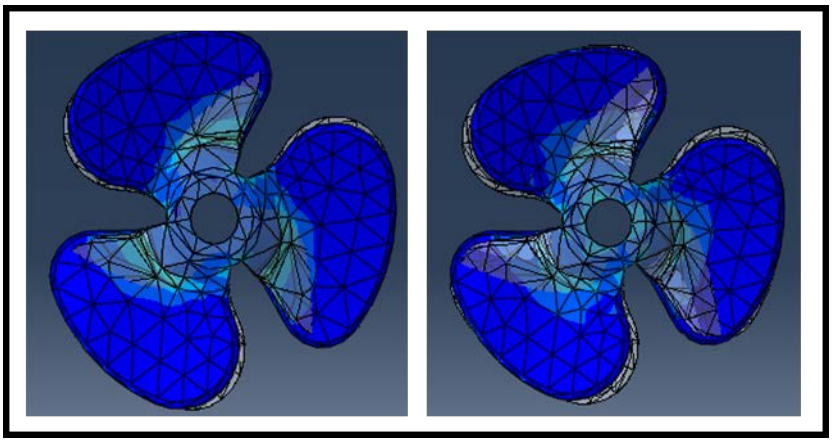

(b)

Figure 4-12. Application example of FBM analysis and 3D orthogonal woven composite structure. (a) Damage initiation and propagation - 2D woven (top) and 3D woven (bottom) and (b) Strain distribution at failure strain - 2D woven (left) and 3D woven (right)

Post forming example is also done with FBM analysis. This method can be used to preform analysis. Figure 4-13 is example of post forming process. In this simulation, simple mandrel is designed and cylindrical braided preform is

used. For mandrel, rigid body property is applied and braided preform property is assumed transverse isotropic carbon fiber without resin. Avoiding numerical problems, resin property is assumed isotropic and having 10^{-6} order modulus as zero value. After combining two part, uniform pressure is applied to outer surface of the model. Figure 4-13(b) is yarn orientation tracing result at outer most curved point. According to deformation, yarn orientation is changed and, due to inner structure radius is smaller than outer parts, that is the reason of angle changed to bigger.

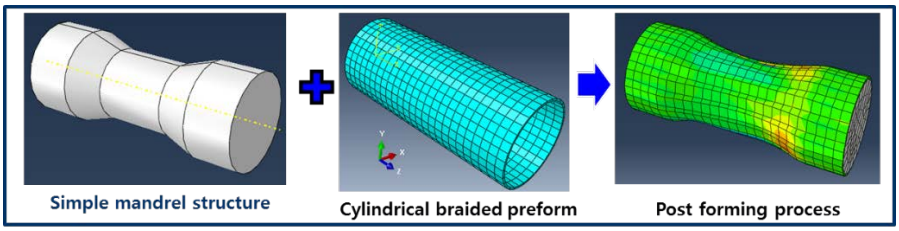

(a)

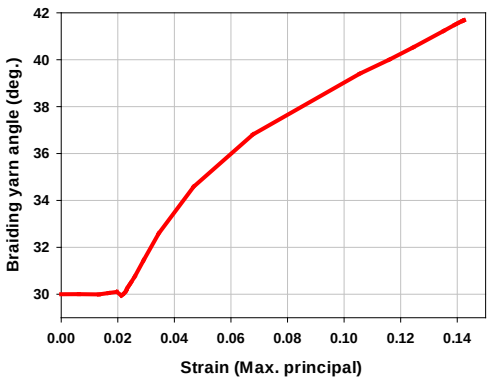

(b)

Figure 4-13. Post forming process with FBM analysis. (a) Example structure simulation and (b) inner yarn orientation change at most curved point

4.4 Summary

FBM analysis method is main idea of this study and it is explained at chapter 2. 3D textile composite fabrication is well researched in many studies, however until it was case by case study was done. In this chapter, using FBM, 3D textile mechanical property analysis was done. 3D braided and orthogonal woven composite samples, which were made at chapter 3, was used for validation. Tensile and bending test was done for characterization of 3D textile composite properties and validation of FBM analysis. The FBM numerical analysis was well predicted 3D textile composite properties and one step analysis can be available. Also 3D composite structure has high performance in strength and toughness behavior, especially, 3D orthogonal woven composite has particular properties on toughness than other textile composites Moreover, according to FBM analysis, inside composite fiber structure change is predicted as yarn orientation change. Damage mode and propagation is also predicted based on Puck's failure criterion. This FBM analysis works is done with commercial finite element analysis software ABAQUS and its user subroutine. Finally, application of these 3D textile composite and FBM analysis is investigated by composite blade analysis example.

Chapter 5. Concluding remarks

Based on previous numerical analysis technics, the new algorithm for prediction of mechanical behavior of 3D textile composite is developed, called fiber based continuum model (FBM). The 3D textile manufacturing process is also developed for 3D braided and orthogonal woven composites.

At first, in chapter 2, FBM analysis model is developed considering fiber orientation in the composites. The model is focused on yarn structure and tracing the orientation of the yarn during deformation. For this, yarn update model is developed with deformation gradient at each increment of numerical analysis step. The yarn path is implemented as polynomial function coordinates with several assumption. Moreover, differential of each coordinates is used for calculating the angle change of the yarn in composites. Based on this structure, stress and strength is computed as stress strain behavior. The elastic property of the composites was calculated using layer model that is considering each yarn part as a sandwich layer. The base parameters are used as fundamental materials as fiber and matrix. Here, the elastic properties is calculated just using rule of mixture and tensor transform. For strength analysis, partial damage and propagation was considered. The failure conditions were obtained by unidirectional composites and tensor transform then used failure criterion on each yarn part and propagation. Puck's criterion is used in this study as 3D failure criterion. This numerical model, that is FBM, is composed as user subroutine in commercial numerical analysis software ABAQUS.

Chapter 3 is about fabrication of 3D textile composites. In this study, 3D five axis braided and orthogonal woven composite is manufactured. For braided composite, the preform of braided structure is made based con four step circular braided machine that is manufactured in the lab. According to manipulation of carrier motion, 4 layer rectangular braided preform is produced. 3D orthogonal woven preform is also made in the laboratory with newly developed 3D weaving jig. In this study, make the jig for continuous 3D weaving process, so even though manufacturing discontinuous sample in this chapter, the mechanism can be used continuous fabrication process. Forming process is also researched with VARTM process. Unidirectional composite is molded with simple pressure molding and braided composite is manufactured with typical VARTM process. However, 3D orthogonal woven composite that is made in this study, has very small fiber volume fraction and cannot be formed with typical VARTM process. Therefore new VARTM process mold and injection condition is researched and optimized. And then the structure modeling of 3D textile is done with textile fabrication software, TEXGEN. Based on this structure model, unit cell analysis is done and it is used for yarn orientation calculation for FBM analysis. Furthermore, the yarn structure is verified with image process as micro CT.

Based on numerical analysis model in chapter 2 and textile composite samples and model in chapter 3, numerical analysis and validation was done. Experimental work of 3D textile composite was done as tensile and bending test. They are fundamental mechanical behavior of structural materials. The numerical analysis was done with FBM analysis and validation with comparing to experimental result. Here, in the numerical analysis, not only stress-strain

behavior is discussed, but also damage mode and propagation of 3D textile composite is considered. Especially, 3D orthogonal woven composite has particular properties on toughness than other textile composites. Moreover, according to FBM analysis, inner composite structure change is predicted as yarn orientation change. Damage mode and propagation is also predicted using Puck's failure criterion. This FBM analysis works is done with commercial finite element analysis software ABAQUS and its user subroutine.

In conclusion, there are new algorithm for continuum analysis for 3D textile composites and its fabrication. For manufacturing part, 3D braided and orthogonal woven composites are fabricated and characterized. These 3D composites have particular properties as high toughness and strength without delamination. And then FBM analysis model is developed and validated with experimental study. The numerical and experimental result shows that particular properties of 3D textile and merits of FBM analysis algorithm.

References

[1] Tan P, Tong L, Steven GP. Modelling for predicting the mechanical properties of textile composites—A review. Composites Part A: Applied Science and Manufacturing. 1997;28(11):903-22.

[2] Adanur S, Liao T. 3D modeling of textile composite preforms. Composites Part B: Engineering. 1998;29(6):787-93.

[3] Ishikawa T, Chou TW. Stiffness and strength behaviour of woven fabric composites. J Mater Sci. 1982;17(11):3211-20.

[4] Ishikawa T, Chou TW. Nonlinear Behavior of Woven Fabric Composites. Journal of Composite Materials. 1983;17(5):399-413.

[5] Hahn HT, Tsai SW. Nonlinear Elastic Behavior of Unidirectional Composite Laminae. Journal of Composite Materials. 1973;7(1):102-18.

[6] Whitney TJ, Chou T-W. Modeling of 3-D Angle-Interlock Textile Structural Composites. Journal of Composite Materials. 1989;23(9):890-911.

[7] Zhang YC, Harding J. A numerical micromechanics analysis of the mechanical properties of a plain weave composite. Computers & Structures. 1990;36(5):839-44.

[8] Naik NK, Shembekar PS. Elastic Behavior of Woven Fabric Composites: I—Lamina Analysis. Journal of Composite Materials. 1992;26(15):2196-225.

[9] Naik NK, Shembekar PS. Elastic Behavior of Woven Fabric Composites: III — Laminate Design. Journal of Composite Materials. 1992;26(17):2522-41.

[10] Naik NK, Ganesh VK. Prediction of on-axes elastic properties of plain weave fabric composites. Composites Science and Technology. 1992;45(2):135-52.

[11] Ganesh VK, Naik NK. Failure Behavior of Plain Weave Fabric Laminates under On-Axis Uniaxial Tensile Loading: I—Laminate Geometry. Journal of Composite Materials. 1996;30(16):1748-78.

[12] Ganesh VK, Naik NK. Failure Behavior of Plain Weave Fabric Laminates under On-Axis Umnaxial Tensile Loading: III—Effect of Fabric Geometry.

Journal of Composite Materials. 1996;30(16):1823-56.
[13] Sankar BV, Marrey RV. A unit-cell model of textile composite beams for predicting stiffness properties. Composites Science and Technology. 1993;49(1):61-9.
[14] Ichihashi H, Hamada H, Ikuta N, Maekawa Z. Finite element analysis of woven fabric composites considering interfacial properties. Composite Interfaces. 1994;2(2):81-94.
[15] Glaessgen EH, Pastore CM, Griffin OH, Birger A. Geometrical and finite element modelling of textile composites. Composites Part B: Engineering. 1996;27(1):43-50.
[16] Cox BN, Carter WC, Fleck NA. A binary model of textile composites—I. Formulation. Acta Metallurgica et Materialia. 1994;42(10):3463-79.
[17] Xu J, Cox BN, McGlockton MA, Carter WC. A binary model of textile composites—II. The elastic regime. Acta Metallurgica et Materialia. 1995;43(9):3511-24.
[18] Whitcomb JD. Iterative global/local finite element analysis. Computers & Structures. 1991;40(4):1027-31.
[19] Whitcomb JD, Woo K. Application of iterative global/local finite-element analysis. Part 1: Linear analysis. Communications in Numerical Methods in Engineering. 1993;9(9):745-56.
[20] Thompson DM, Griffin OH. Verification of a 2-D to 3-D Global/Local Finite Element Method for Symmetric Laminates. Journal of Reinforced Plastics and Composites. 1992;11(8):910-31.
[21] Woo K, Whitcomb J. Global/Local Finite Element Analysis for Textile Composites. Journal of Composite Materials. 1994;28(14):1305-21.
[22] Chapman C, Whitcomb J. Effect of Assumed Tow Architecture on Predicted Moduli and Stresses in Plain Weave Composites. Journal of Composite Materials. 1995;29(16):2134-59.
[23] Whitcomb J, Srirengan K. Effect of various approximations on predicted progressive failure in plain weave composites. Composite Structures.

1996;34(1):13-20.
[24] Chang F-K, Chang K-Y. A Progressive Damage Model for Laminated Composites Containing Stress Concentrations. Journal of Composite Materials. 1987;21(9):834-55.
[25] Dasgupta A, Agarwal RK, Bhandarkar SM. Three-dimensional modeling of woven-fabric composites for effective thermo-mechanical and thermal properties. Composites Science and Technology. 1996;56(3):209-23.
[26] Pastore CM, Gowayed Y. A self-consistent fabric geometry model: modification and application of a fabric geometry model to predict the elastic properties of textile composites. ASTM J Compos Technol Res(USA). 1994;16(1):32-6.
[27] Vandeurzen P, Ivens J, Verpoest I. A three-dimensional micromechanical analysis of woven-fabric composites: II. Elastic analysis. Composites Science and Technology. 1996;56(11):1317-27.
[28] Sun CT, Vaidya RS. Prediction of composite properties from a representative volume element. Composites Science and Technology. 1996;56(2):171-9.
[29] Callus PJ, Mouritz AP, Bannister MK, Leong KH. Tensile properties and failure mechanisms of 3D woven GRP composites. Composites Part A: Applied Science and Manufacturing. 1999;30(11):1277-87.
[30] Rudov-Clark S, Mouritz AP. Tensile fatigue properties of a 3D orthogonal woven composite. Composites Part A: Applied Science and Manufacturing. 2008;39(6):1018-24.
[31] Ma C-L, Yang J-M, Chou T-W. Elastic stiffness of three-dimensional braided textile structural composites. ASTM special technical publication. 1986(893):404-21.
[32] Yang J-M, Ma C-L, Chou T-W. Fiber Inclination Model of Three-Dimensional Textile Structural Composites. Journal of Composite Materials. 1986;20(5):472-84.
[33] Naik RA. Failure Analysis of Woven and Braided Fabric Reinforced

Composites. Journal of Composite Materials. 1995;29(17):2334-63.
[34] Byun J-H. The analytical characterization of 2-D braided textile composites. Composites Science and Technology. 2000;60(5):705-16.
[35] Quek SC, Waas AM, Shahwan KW, Agaram V. Analysis of 2D triaxial flat braided textile composites. International Journal of Mechanical Sciences. 2003;45(6–7):1077-96.
[36] Ayranci C, Carey J. 2D braided composites: A review for stiffness critical applications. Composite Structures. 2008;85(1):43-58.
[37] Shokrieh MM, Mazloomi MS. An analytical method for calculating stiffness of two-dimensional tri-axial braided composites. Composite Structures. 2010;92(12):2901-5.
[38] Naik RA, Ifju PG, Masters JE. Effect of Fiber Architecture Parameters on Deformation Fields and Elastic Moduli of 2-D Braided Composites. Journal of Composite Materials. 1994;28(7):656-81.
[39] Huang Zm. The mechanical properties of composites reinforced with woven and braided fabrics. Composites Science and Technology. 2000;60(4):479-98.
[40] Zeng T, Wu L-z, Guo L-c. Mechanical analysis of 3D braided composites: a finite element model. Composite Structures. 2004;64(3–4):399-404.
[41] Ivanov DS, Baudry F, Van Den Broucke B, Lomov SV, Xie H, Verpoest I. Failure analysis of triaxial braided composite. Composites Science and Technology. 2009;69(9):1372-80.
[42] Hinton MJ, Kaddour AS, Soden PD. Chapter 1.1 - The world-wide failure exercise: Its origin, concept and content. In: Soden MJHSKD, editor. Failure Criteria in Fibre-Reinforced-Polymer Composites. Oxford: Elsevier; 2004. p. 2-28.
[43] Eckold GC. Chapter 3.2 - Failure criteria for use in the design environment*. In: Soden MJHSKD, editor. Failure Criteria in Fibre-Reinforced-Polymer Composites. Oxford: Elsevier; 2004. p. 121-39.
[44] Camanho PP. Failure criteria for fibre-reinforced polymer composites.

Secção de Mecânica Aplicada, Departamento de Engenharia Mecânica e Gestão Industrial, Faculdade de Engenharia da Universidade do Porto. 2002.
[45] Hinton MJ, Soden PD. Predicting failure in composite laminates: the background to the exercise. Composites Science and Technology. 1998;58(7):1001-10.
[46] Sun CT, Quinn, B.J., Tao, J. and Oplinger, D.W. Comparative Evaluation of Failure Analysis Methods for Composite Laminates. NASA. 1996;DOT/FAA/AR-95/109.
[47] Tsai SW, Wu EM. A General Theory of Strength for Anisotropic Materials. Journal of Composite Materials. 1971;5(1):58-80.
[48] Hart-Smith LJ. Predictions of the original and truncated maximum-strain failure models for certain fibrous composite laminates. Composites Science and Technology. 1998;58(7):1151-78.
[49] Tsai SW. Strength Characteristics of Composite Materials. DTIC Document; 1965.
[50] Azzi VD, Tsai SW. Anisotropic strength of composites. Experimental Mechanics. 1965;5(9):283-8.
[51] Hoffman O. The Brittle Strength of Orthotropic Materials. Journal of Composite Materials. 1967;1(2):200-6.
[52] Chamis CC. Failure Criteria for Filamentary Composites. DTIC Document; 1969.
[53] Hashin Z, Rotem A. A Fatigue Failure Criterion for Fiber Reinforced Materials. Journal of Composite Materials. 1973;7(4):448-64.
[54] Hashin Z. Failure Criteria for Unidirectional Fiber Composites. Journal of Applied Mechanics. 1980;47(2):329-34.
[55] Puck A, Schürmann H. FAILURE ANALYSIS OF FRP LAMINATES BY MEANS OF PHYSICALLY BASED PHENOMENOLOGICAL MODELS1. Composites Science and Technology. 1998;58(7):1045-67.
[56] Yamada SE, Sun CT. Analysis of Laminate Strength and Its Distribution. Journal of Composite Materials. 1978;12(3):275-84.

[57] Kroll L, Hufenbach W. Physically Based Failure Criterion for Dimensioning of Thick-Walled Laminates. Applied Composite Materials. 1997;4(5):321-32.
[58] Zinoviev PA, Grigoriev SV, Lebedeva OV, Tairova LP. The strength of multilayered composites under a plane-stress state. Composites Science and Technology. 1998;58(7):1209-23.
[59] Orifici AC, Herszberg I, Thomson RS. Review of methodologies for composite material modelling incorporating failure. Composite Structures. 2008;86(1–3):194-210.
[60] Chang F-K, Lessard LB. Damage Tolerance of Laminated Composites Containing an Open Hole and Subjected to Compressive Loadings: Part I—Analysis. Journal of Composite Materials. 1991;25(1):2-43.
[61] Pinho ST, Dàvila CG, Camanho PP, Iannucci L, Robinson P. Failure models and criteria for FRP under in-plane or three-dimensional stress states including shear non-linearity. NASA Technical Memorandum. 2005;213530:18.
[62] Maimí P, Camanho PP, Mayugo JA, Dávila CG. A continuum damage model for composite laminates: Part II – Computational implementation and validation. Mechanics of Materials. 2007;39(10):909-19.
[63] Lee JD. Three dimensional finite element analysis of damage accumulation in composite laminate. Computers & Structures. 1982;15(3):335-50.
[64] Christensen RM. Stress based yield/failure criteria for fiber composites. International Journal of Solids and Structures. 1997;34(5):529-43.
[65] Shahid I, Chang F-K. An Accumulative Damage Model for Tensile and Shear Failures of Laminated Composite Plates. Journal of Composite Materials. 1995;29(7):926-81.
[66] Ladeveze P, LeDantec E. Damage modelling of the elementary ply for laminated composites. Composites Science and Technology. 1992;43(3):257-67.
[67] Wisnom M, Hill G, Jones M. Through thickness failure prediction of

composite structural elements. Proceedings of the 13th international conference on composite materials, Beijing, China Paper2001.
[68] Talreja R. Damage mechanics of composite materials: Elsevier; 1994.
[69] Ochoa OO, Engblom JJ. Analysis of progressive failure in composites. Composites Science and Technology. 1987;28(2):87-102.
[70] Brewer JC, Lagace PA. Quadratic Stress Criterion for Initiation of Delamination. Journal of Composite Materials. 1988;22(12):1141-55.
[71] Tong L. An Assessment of Failure Criteria to Predict the Strength of Adhesively Bonded Composite Double Lap Joints. Journal of Reinforced Plastics and Composites. 1997;16(8):698-713.
[72] Zhang X. Impact damage in composite aircraft structures-experimental testing and numerical simulation. Proceedings of the Institution of Mechanical Engineers, Part G: Journal of Aerospace Engineering. 1998;212(4):245-59.
[73] Goyal VK, Johnson ER, Dávila CG, Jaunky N. An irreversible constitutive law for modeling the delamination process using interface elements: ICASE, NASA Langley Research Center; 2002.
[74] Puck A, Schürmann H. Failure analysis of FRP laminates by means of physically based phenomenological models. Composites Science and Technology. 2002;62(12–13):1633-62.
[75] Lessard LB, Shokrieh MM. Two-Dimensional Modeling of Composite Pinned-Joint Failure. Journal of Composite Materials. 1995;29(5):671-97.
[76] Shokrieh MM, Lessard LB. Progressive Fatigue Damage Modeling of Composite Materials, Part I: Modeling. Journal of Composite Materials. 2000;34(13):1056-80.
[77] Naderi M, Maligno AR. Fatigue life prediction of carbon/epoxy laminates by stochastic numerical simulation. Composite Structures. 2012;94(3):1052-9.
[78] Du G-W, Ko FK. Unit Cell Geometry of 3-D Braided Structures. Journal of Reinforced Plastics and Composites. 1993;12(7):752-68.
[79] Ahn H, Kim KJ, Park SY, Huh JE, Kim HJ, Yu W-R. 3D braid scaffolds for regeneration of articular cartilage. Journal of the Mechanical Behavior of

Biomedical Materials. 2014;34:37-46.
[80] Miravete A, Bielsa JM, Chiminelli A, Cuartero J, Serrano S, Tolosana N, et al. 3D mesomechanical analysis of three-axial braided composite materials. Composites Science and Technology. 2006;66(15):2954-64.
[81] Zuorong C, Dechao Z, Lu M, Ye L. Evaluation of elastic properties of 3-D (4-step) regular braided composites by a homogenisation method. Composite Structures. 1999;47(1–4):477-82.
[82] Gu B, Xu J. Finite element calculation of 4-step 3-dimensional braided composite under ballistic perforation. Composites Part B: Engineering. 2004;35(4):291-7.
[83] Maligno AR, Warrior NA, Long AC. Effects of interphase material properties in unidirectional fibre reinforced composites. Composites Science and Technology. 2010;70(1):36-44.

Korean Abstract

섬유강화 복합재료는 현재 군사, 항공 및 여러 산업 분야에서 활용되고 있으며 다양한 첨단 구조재료로서 각광받고 있다. 이와 같은 다양한 수요를 만족하기 위해 구조 설계 및 복합재료의 제조 방법에 대한 많은 연구가 수행되어왔다. 또한 복합재료의 구조적 단점을 해결하기 위해 삼차원 섬유 강화 복합재료의 연구가 진행되고 있으며, 그 구조적 특징으로 인해 단위 구조체를 바탕으로 한 연구가 많이 진행 되었으며 이를 기반으로 하여 구조재료의 해석을 진행하는 단계로 활용되고 있다. 본 연구에서는 이와 같은 복잡한 다단계 해석 과정을 간소화하고 변형에 따른 구조적인 변화에서 오는 해석적 변수를 고려하기 위해 섬유 기반 연속체 모델을 개발하고 검증을 진행하였다.

해당 해석 모델, Fiber based model(FBM) 은 삼차원 복합재료의 물성 해석을 위해 복합재료 내부 섬유 구조를 반영한 연속체 역학 기반의 유한 요소 법을 통해 복합재료의 연속 거동을 해석하는 것이 특징으로 각 구조체의 반복단위를 설정하고 이에 해당하는 섬유 구조를 연속적으로 갱신하여 해석을 진행하는 것이 특징이다. FBM은 이와 같은 특징으로 인해 섬유와 수지의 기본 강성 및 강도를 바탕으로 삼차원 구조체의 물성을 하나의 해석 프로세스로 해석 가능한 알고리즘을 가지고 있다. 해석 과정에서는 섬유의 구조를 모사하기 위해 각 섬유 파트의 방향성을 다항 함수를 통해 근사하였으며, 각 부분의 물성을 텐서 변환을 통해 예측하고, Puck’s criterion에 기반하여 부분 파손 및 진행과 파손 모드, 그리고 최종 파손에 대한 해석을 진행하였다. 이를 통해 섬유 복합재료 구조를 각 파트로 나누어 계산하여 특정 면의 부분 파손 거동을 추적할 수 있고, 해당 파손이 어떤 모드로 진행 중인지 예측할 수 있다

다음 장에서는 3차원 섬유 강화 복합재료의 활용 가능성 모색과 해석 알고리즘의 검증을 위해 실제 복합재료 시편을 제작 하였으며, 본 연구에서는 편조 구조와 삼차원 직조 구조의 시편을 제작하고 시험을 진행하였다. 편조 구조의 경우 수직 배향 사를 포함한 5축 기반의 편조 구조를 제작하였으며, 삼차원 직조 구조는 Orthogonal woven 구조를 기반으로 한 구조를 제작하였다. 또한 시편 제작을 위해 삼차원 편조와 직조 구조를 제조를 위한 연속 공정에 응용 가능한 직조 및 성형 프로세스를 개발하였다.

최종적으로 이와 같은 삼차원 복합재료 구조들의 물성을 FBM 모델을 통해 해석을 진행하고 이를 비교 검증하였으며, 기존 단위 구조체 모델과 비교하여 충분한 가능성과 정확성을 확보하였다. 특히 삼차원 직조 구조의 경우 구조 해석에 있어 기존의 해석 모델들과 달리 구조체에서의 변형에 따른 응력 분포 및 파손에 대한 해석을 진행하였으며 이를 통해 다양한 구조적 요인의 특성 해석도 가능할 것으로 사료된다. 또한 변형이 큰 경우에도 복합재료 구조의 내부 변형을 고려하여 전체물성 및 파손에 대한 해석을 할 수 있으며, 구조변화에 따른 물성 예측을 가능하게 할 뿐만 아니라 다양한 삼차원 구조 섬유강화 복합재료에 활용 가능할 것으로 기대된다.

핵심어: 섬유강화 복합재료, 수치해석, 구조해석, 삼차원 복합재료, 섬유기반 연속체 모델

학번: 2010-30177